

# Mathematical modelling of dynamic adaptive tumour-induced angiogenesis: Clinical implications and therapeutic targeting strategies

Steven R. McDougall<sup>a,\*</sup>, Alexander R.A. Anderson<sup>b</sup>, Mark A.J. Chaplain<sup>b</sup>

<sup>a</sup>*Institute of Petroleum Engineering, Heriot-Watt University, Edinburgh EH14 4AS, Scotland, UK*

<sup>b</sup>*The SIMBIOS Centre, Division of Mathematics, University of Dundee, Dundee DD1 4HN, Scotland, UK*

Received 11 November 2005; received in revised form 20 December 2005; accepted 26 December 2005

Available online 17 February 2006

## Abstract

Angiogenesis, the growth of a network of blood vessels, is a crucial component of solid tumour growth, linking the relatively harmless avascular growth phase and the potentially fatal vascular growth phase. As a process, angiogenesis is a well-orchestrated sequence of events involving endothelial cell migration, proliferation; degradation of tissue; new capillary vessel (sprout) formation; loop formation (anastomosis) and, crucially, blood flow through the network. Once there is blood flow associated with the nascent network, the subsequent growth of the network evolves both temporally and spatially in response to the combined effects of angiogenic factors, migratory cues via the extracellular matrix and perfusion-related haemodynamic forces in a manner that may be described as both *adaptive* and *dynamic*. In this paper we present a mathematical model which *simultaneously* couples vessel growth with blood flow through the vessels—*dynamic adaptive tumour-induced angiogenesis* (DATIA). This new mathematical model presents a theoretical and computational investigation of the process and highlights a number of important new targets for therapeutic intervention. In contrast to earlier flow models, where the effects of perfusion (blood flow) were essentially evaluated a posteriori, i.e. after generating a hollow network, blood flow in the model described in this paper has a direct impact *during* capillary growth, with radial adaptations and network remodelling occurring as *immediate* consequences of primary anastomoses. Capillary network architectures resulting from the dynamically adaptive model are found to differ radically from those obtained using earlier models.

The DATIA model is used to examine the effects of changing various physical and biological model parameters on the developing vascular architecture and the delivery of chemotherapeutic drugs to the tumour. Subsequent simulations of chemotherapeutic treatments under different parameter regimes lead to the identification of a number of new therapeutic targets for tumour management.

© 2006 Elsevier Ltd. All rights reserved.

**Keywords:** Angiogenesis; Blood flow; Capillary remodelling

## 1. Introduction

Angiogenesis is the process by which new blood vessels develop from an existing vasculature, through endothelial cell sprouting, proliferation and fusion (Risau, 1997). Adult endothelial cells (ECs) are normally quiescent and, apart from certain developmental processes (e.g. embryogenesis) and wound healing, angiogenesis is generally a pathological process implicated in arthritis (Walsh, 1999),

some eye diseases, and solid tumour development, invasion and metastasis (Folkman, 1995). Tumour-induced angiogenesis is believed to occur when a small avascular tumour exceeds some critical diameter (~2 mm), above which normal tissue vasculature is no longer able to support its growth (Folkman, 1971). At this stage, the tumour cells lacking nutrients and oxygen become hypoxic. This is assumed to trigger cellular release of tumour angiogenic factors (TAFs) (Folkman and Klagsbrun, 1987), which start to diffuse into the surrounding tissue and approach the ECs of nearby blood vessels. Endothelial cells subsequently respond to the TAF concentration gradient by forming sprouts, dividing and migrating towards the tumour (Ausprunk and Folkman, 1977; Sholley et al.,

\*Corresponding author. Tel.: +44 131 451 3166; fax: +44 131 451 3127.

E-mail addresses: [steve.mcdougall@pet.hw.ac.uk](mailto:steve.mcdougall@pet.hw.ac.uk) (S.R. McDougall), [anderson@maths.dundee.ac.uk](mailto:anderson@maths.dundee.ac.uk) (A.R.A. Anderson), [chaplain@maths.dundee.ac.uk](mailto:chaplain@maths.dundee.ac.uk) (M.A.J. Chaplain).

1984). It takes approximately 10 to 21 days for the growing network to link the tumour to the parent vessel (Gimbrone et al., 1974; Ausprunk and Folkman, 1977; Muthukruppan et al., 1982), and this vascular connection subsequently provides all the nutrients and oxygen required for continued tumour growth. An excellent summary of all the key processes involved in angiogenesis can be found in the comprehensive review article of Paweletz and Knierim (1989). More recent individual summaries of selected components of angiogenesis can be found in the papers of Carmeliet (2003), Cleaver and Melton (2003), Ferrara et al. (2003), Jain (2003), Pugh and Ratcliffe (2003), Rafii and Lyden, (2003), Ylä-Herttuala and Alitalo (2003).

At this stage in tumour development, chemotherapy treatments can be administered and tumour cells can be specifically targeted via the newly developed vasculature. However, although most of the drugs used to date have proven to be successful on small animals (e.g. mice), their efficiency in humans remains highly variable from one patient to another. One of the main reasons suggested to explain such variability is the issue of drug delivery to the tumour—it is thought possible that most of the drug can bypass large areas of the target (Jain, 1987, 1988). In light of this, more theoretical models are being developed in an attempt to better understand vascular architecture and microcirculatory dynamics (Secomb, 1995; Baish et al., 1996; El-Kareh and Secomb, 1997; Quarteroni et al., 2000; Godde and Kurz, 2001; Krenz and Dawson, 2002).

Over the past 10 years or so, there has been a lot of interest in the mathematical modelling of tumour-induced angiogenesis. The modelling has focussed mainly on the key role played by ECs during the formation of the new blood vessels. These models have considered the endothelial cell proliferative and migratory response to different signalling cues, including those associated with the soluble and diffusible angiogenic factors secreted by the cancer cells of the solid tumour itself, as well as those arising from insoluble molecules present in the extracellular matrix (ECM) (e.g. fibronectin). These key interactions of the ECs with angiogenic factors and macromolecules of the matrix have typically led to systems of nonlinear PDEs describing the migration of capillary vessels from a parent vessel through the ECM towards the solid tumour. Some of these models have contained a discrete element, allowing the formation of individual capillary vessels to be examined in detail by tracking the progress of individual ECs. Key papers in this area include the works of Stokes and Lauffenburger (1991), Orme and Chaplain (1997), Olsen et al. (1997), Anderson and Chaplain (1998), Levine et al. (2001), Plank and Sleeman (2004). An excellent comprehensive overview of the modelling done in this area can be found in the review paper of Mantzaris et al. (2004).

By contrast, blood flow modelling in a tumour-induced (micro) capillary network has only been considered relatively recently in papers by McDougall et al. (2002), Alarcon et al. (2003) and Stéphanou et al. (2005, 2006). Blood is a complex fluid, the rheological properties of

which lead to interesting feedback mechanisms during perfusion. For example, shear stresses generated within the capillary network by the flowing blood strongly influence vessel adaptation and network remodelling (Lehoux and Tedgui, 1998; Taber, 1998; Quick et al., 2000; Godde and Kurz, 2001; Fisher et al., 2001). These shear stresses are, in turn, affected by blood viscosity, the distribution of which depends upon a non-uniform distribution of haematocrit (volume fraction of red blood cells contained in the blood) within the host vasculature (the Fåhræus effect). However, the distribution of haematocrit itself depends upon the spatial architecture of the underlying network and so the feedback is established, “the modelling loop is closed”, so to speak. Blood rheology and its influence on the remodelling of microvascular networks have been extensively studied by Pries et al. (1998, 2001a,b) both experimentally and theoretically. From these studies Pries and co-workers have formulated a model for vascular adaptation incorporating a number of feedback mechanisms. They have demonstrated that the basic requirement for the generation of stable vascular structures involves a combination of both haemodynamic and metabolic stimuli.

In the work of McDougall et al. (2002), flow simulations through the vascular networks were performed to investigate the efficiency of chemotherapy treatments as they passed from a nearby parent vessel to the tumour surface via a network of capillary vessels. These vessels had been stimulated to grow by chemical factors secreted by the tumour cells themselves (i.e. tumour-induced angiogenesis). The capillary vessels were generated from an angiogenesis model of Anderson and Chaplain (1998)—the growth of the vascular network was described by a discrete formulation of the set of governing partial differential equations and the migration of each individual endothelial cell was traced as it emerged from a parent vessel. Endothelial cells migrated via a biased random walk process with three main components of movement: (i) random motility, (ii) chemotaxis in response to a generic TAF released by the tumour cells, and (iii) haptotaxis in response to fibronectin gradients generated in the ECM as the ECs migrate (a combination of degradation and production). Flow modelling techniques used previously in the context of petroleum engineering to model the flow of water, oil and gas through the interstices of a porous rock (McDougall and Sorbie, 1997) were adapted to model blood and drug flow through these microvascular networks. Although blood was rather crudely considered to be a Newtonian fluid in this early work, results from McDougall et al. (2002) highlighted two important effects that could be responsible for the failure of some therapy regimes. First, it was found that a considerable amount of the drug injected into the parent vessel simply by-passed the tumour by way of the highly interconnected capillary network. The second effect related to the dilution of the drug as it became dispersed throughout the tumour-induced vasculature: the concentration of any drug reaching the tumour became so dilute as to have little effect on the tumour cells.

Simulations were then performed to investigate ways of reducing these two detrimental phenomena and thereby optimize the drug uptake by the tumour. Increasing the mean capillary radius of the capillary bed and/or decreasing the blood viscosity both led to a significant increase in the drug uptake. Although these results were interesting from a qualitative perspective, this early model was somewhat naïve, with blood perfusion modelled as the flow of a Newtonian fluid through rigid cylindrical capillaries.

The paper of Stéphanou et al. (2005) extended the work of McDougall et al. (2002) by examining how the removal of certain capillaries affected the distribution of blood flow in the system. Capillary pruning algorithms were designed to reflect how different anti-vascular and anti-angiogenic drugs were thought to operate in vivo. Simulations demonstrated that drug uptake could be increased by up to 130% via the random removal of vessels and this suggested the possibility of developing a new cancer treatment strategy, viz, coupling the administration of an anti-angiogenic drug (to preliminarily optimize the vasculature) prior to chemotherapy treatment (thereby ensuring maximum delivery). In this paper modelling and simulations were also carried out on fully three-dimensional networks.

Vascular adaptation processes have also been recently incorporated into models comprising regular capillary networks (Alarcon et al., 2003) and capillary networks originating from tumour-induced angiogenesis (Stéphanou et al., 2006). The aim of the work of Alarcon et al. (2003) was to model the oxygen distribution within a two-dimensional regular hexagonal network of blood vessels and to determine its influence on the dynamics of a colony of normal and cancerous cells. Results from computational simulations of the model produced inhomogeneous distributions of haematocrit and oxygen tension and highlighted the important role played by hypoxic cells during tumour invasion. The work of Stéphanou et al. (2006) modelled an adaptive vasculature associated with tumour-induced angiogenesis and considered how this adaptive remodelling affected the supply of oxygen and drugs to the tumour cells. However, in both papers, the flow modelling was carried out a posteriori, either after simply generating a hexagonal hollow vessel network *a mano* (Alarcon et al., 2003) or after an initial cell migration model had produced a hollow vessel network (Stéphanou et al., 2006).

The aim of the current paper is to implement a number of significant improvements in the modelling approach by considering the flow of a *non-Newtonian fluid* in a *dynamic adaptive* network, i.e. a network that evolves both spatially and temporally in response to its associated flow distribution. We present results corresponding to a number of different stages in the formulation of what we call our *dynamic adaptive tumour-induced angiogenesis* (DATIA) model.

The model of DATIA presented in this paper begins with an implementation of a formulation of endothelial cell

migration at the capillary sprout tips that explicitly takes into account the important function of matrix degrading enzymes (such as matrix metalloproteinases, MMPs; urokinase plasminogen activators, uPAs) during angiogenesis in the absence of flow (Levine et al., 2002; Lolas, 2003). We explicitly incorporate mediation in vessel growth via ECM proteolysis by specific enzymes produced by ECs. A number of recent publications have demonstrated the importance of enzymes from the MMP family and their involvement in the regulation of the various stages of the angiogenic process (Davis et al., 2000; Yan et al., 2000; Hidalgo and Eckhardt, 2001; Sternlicht and Werb, 2001). These MMPs are involved in the migration of ECs within the ECM, EC proliferation, and the remodelling of the basement membrane of newly formed vessels. Their importance is such that these proteinases and their regulation form new targets for cancer treatment. As our ultimate goal is to propose a global modelling framework within which to further investigate new treatments, it is important to incorporate explicitly the MMP effect into the modelling. Another key aspect of the MMP issue relates to their effect on transmural transport—tumour vascular networks are very leaky and proteolytic activity plays a vital part in the breaching of non-mature capillary membranes by ECs during sprout formation. Although we will not take vessel leakiness into account in the present paper, this aspect is currently under investigation in an attempt to describe drug diffusion through the tumour tissue itself. Matrix degrading enzymes also play a key role in the invasion of tissue by cancer cells, something which is closely tied in with tumour-induced angiogenesis (Anderson et al., 2000; Lolas, 2003; Anderson, 2005).

The main aim of this paper is to investigate the impact of blood perfusion *during* angiogenesis and the paper continues with a discussion of a series of models related to capillary flow and vessel remodelling. Whilst previous approaches by McDougall et al. (2002) and Stéphanou et al. (2005) have made the assumptions of constant blood viscosity and invariable vessel radii, and other work by Alarcon et al. (2003) and Stéphanou et al. (2006) has considered remodelling of hollow capillary networks a posteriori, the modelling formulation in this current paper is extended to account for variable blood viscosity and evolving capillary radii coupled directly to the network as it is growing. The model considers a number of stimuli affecting vessel diameter that account for the influence of the wall shear stress (WSS), the intravascular pressure, and a metabolic mechanism depending on the blood haematocrit. In addition, the angiogenesis model of Anderson and Chaplain (1998), where sprout branching depended only upon local TAF concentration, is extended here to take into account the important feature of shear-stress-induced capillary sprouting and branching. Network architectures are produced that adapt dynamically through adjuvant branching of vessels experiencing high shear stresses during perfusion. The flow induces additional branching, resulting in topological perturbations in the developing architecture

that become magnified during successive growth periods. These differences in network structure subsequently alter the distribution of flow (and hence shear stress) throughout the vascular bed and so it is the additional branching mechanism that effectively couples the migration and flow models.

Computational simulation results are presented corresponding to a number of different stages in the formulation of the full DATIA model. The simulation results are presented stage-by-stage in such a way as to show the evolution of the model—this allows the effect of each of the model components to be assessed individually and facilitates direct comparison with previous work. The next section begins with a simulation demonstrating the effect of explicitly incorporating matrix degrading enzyme (MDE) activity into the migration model. At this stage, no flow/remodelling is considered and only sprout branching at the vessel tips is allowed. Subsequent results incorporating flow show the impact of dynamic remodelling and shear-induced vessel branching upon global network architecture. Next, a number of key physical and biochemical parameters are varied in the model to assess their effect upon the network architecture. Finally, in order to quantify the efficiency of these different networks in carrying blood-borne material (e.g. nutrients, drugs) to the tumour, a series of simulations involving the continuous infusion of a “passive tracer-drug” is described. In doing so, some insights are offered into the evolution of chemotherapeutic agents during treatment and a number of new therapeutic targets for tumour management are subsequently identified, thus providing a rational biomechanical basis for an effect which has been known for over 30 years (Salsbury et al., 1970; Le Serve and Hellmann, 1972). The paper concludes with a discussion section summarising all the main results and offering directions for future model development and study.

## 2. A modelling framework for DATIA

Although the ultimate aim of the work presented in this paper is to produce a model of angiogenesis that couples cell migration with blood flow, it will first be beneficial to examine each of these components in isolation.

### 2.1. A model of hollow capillary vessel formation via endothelial cell migration

The model of endothelial cell migration used here describes how capillary sprouts emerging from a parent vessel migrate towards a tumour, leading to the formation of a vascular network that supplies nutrients for continued development. The model is inspired by the tumour-induced angiogenesis model initially proposed by Anderson and Chaplain (1998). The model assumes that ECs at the tips of the new capillary sprouts (vessels) migrate through (i) random motility, (ii) chemotaxis in response to TAF released by the tumour, and (iii) haptotaxis in response

to fibronectin (FN) gradients in the ECM. If we denote by  $n$  the endothelial cell density per unit area, then the (non-dimensional) equation describing endothelial cell conservation is given by

$$\frac{\partial n}{\partial t} = \overbrace{D\nabla^2 n}^{\text{random}} - \overbrace{\nabla \cdot (\chi(c)n\nabla c)}^{\text{chemotaxis}} - \overbrace{\rho\nabla \cdot (n\nabla f)}^{\text{haptotaxis}}. \quad (1)$$

The chemotactic migration is characterized by the function  $\chi(c) = \chi/(1 + \delta c)$ , which reflects the decrease in chemotactic sensitivity with increased TAF concentration. The coefficients  $D$ ,  $\chi$  and  $\rho$  characterize the random, chemotactic and haptotactic cell migration, respectively (details of the scalings used are given in Section 2.4 and full details of the non-dimensionalization can be found in Anderson and Chaplain (1998)).

TAFs and FN bind to specific membrane receptors on ECs and subsequently trigger molecular cascades inside the ECs, activating cell migratory machinery. One consequence of this activation process is the production by the cells of a MDE, which enhances the attachment of the cells to fibronectin contained in the ECM. The ECs are consequently able to exert the traction forces required to propel themselves during migration. In the earlier model of Anderson and Chaplain (1998), endothelial cell densities and their global influence on TAF and FN concentrations were considered in a continuous formulation. Here, we choose to focus on local effects and consider the influence of each individual cell on its local environment. In order to achieve this, the displacement of each individual endothelial cell, located at the tips of growing sprouts, is given by the discretized form of the endothelial cell mass conservation equation (1). The migration of each cell is consequently determined by a set of normalized coefficients emerging from this equation, which relate to the likelihood of the cell remaining stationary ( $P_0$ ), or moving left ( $P_1$ ), right ( $P_2$ ), up ( $P_3$ ) or down ( $P_4$ ) (see Fig. 1 and Anderson and Chaplain (1998) for more details):

$$n_{l,m}^{q+1} = n_{l,m}^q P_0 + n_{l+1,m}^q P_1 + n_{l-1,m}^q P_2 + n_{l,m+1}^q P_3 + n_{l,m-1}^q P_4,$$

where  $l$  and  $m$  are positive parameters which specify the position of the endothelial cell on the two-dimensional spatial grid, i.e.  $x = l\Delta x$  and  $y = m\Delta y$  and time discretization is represented by  $t = q\Delta t$ . These coefficients  $P_0$ – $P_4$  incorporate the effects of random, chemotactic and haptotactic movement and depend upon the local chemical environment (FN and TAF concentrations).

The model is then given by the following set of equations:

$$\begin{aligned} \frac{\partial c}{\partial t} &= -\eta n_k c, \\ \frac{\partial f}{\partial t} &= \beta n_k - \gamma m f, \\ \frac{\partial m}{\partial t} &= \alpha n_k + \varepsilon \nabla^2 m - \nu m, \end{aligned} \quad (2)$$

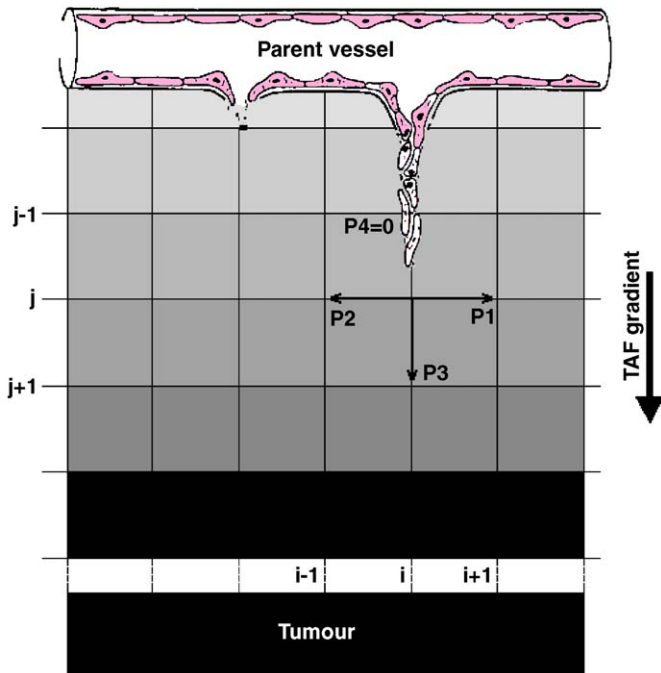


Fig. 1. Schematic diagram of a section of the two-dimensional grid used in the numerical computation procedure illustrating how the process of the migration of tip ECs, and hence capillary sprout growth, is taken into account in the simulations. At each node, the sprout tip can grow in three possible directions in two-dimensional (and five possible directions in three dimensional).

where  $c$  represents the TAF concentration,  $f$  the FN concentration,  $m$  the MDE density and  $n_k$  a Boolean value (1 or 0) that indicates the presence or absence of an endothelial cell at a given position. The parameters  $\beta$  and  $\alpha$  characterize the production rate by an individual endothelial cell of FN and MDE, respectively, and  $\eta$  its TAF consumption rate. The major difference with the earlier model is that degradation of fibronectin  $f$ , characterized by the coefficient  $\gamma$ , no longer depends directly on the endothelial cell density  $n$ . This now depends upon the MDE density  $m$  produced by each individual endothelial cell  $n_k$  at rate  $\alpha$ . (Anderson et al., 2000; Levine et al., 2001; Lolas, 2003; Anderson, 2005). The MDF once produced, diffuses locally with diffusion coefficient  $\varepsilon$ , and is spontaneously degraded at a rate  $\nu$ . Proliferation of the ECs at the capillary tips and branching at capillary tips are implemented in the model at the discrete level. Using the above model it is possible to generate “hollow” capillary networks which are structurally similar to those observed experimentally (Gimbrone et al., 1974; Muthukkaruppan et al., 1982).

## 2.2. Modelling blood perfusion in the developing capillary network

### 2.2.1. Flow through a connected network

Although the main aim of this paper is to investigate the impact of blood perfusion during angiogenesis, we will

introduce our treatment of flow modelling by describing a series of examples of network transport and vessel remodelling that are initially de-coupled from the capillary growth processes. Previous approaches by McDougall et al. (2002) and Stéphanou et al. (2005) had made the rather limiting assumptions of invariant blood viscosity and constant capillary radius, whereas, in reality, biological structures tend to exhibit some degree of compliance and blood is a non-Newtonian fluid. Here, we extend the earlier formulation to account for variable blood viscosity and evolving capillary vessels that may either dilate or constrict both spatially and temporally. We are minded of the words of D’Arcy Thompson, “*We rely once more on Poiseuille’s Law... but we have also to account for the blood itself.*” (Thompson, 1917).

In order to calculate flow within the entire interconnected network of capillaries, it is first necessary to decide upon a local relationship between the pressure gradient  $\Delta P$  and flow  $Q$  at the scale of a single capillary element of length  $L$  and radius  $R$ . Such a relationship in the case of a non-Newtonian fluid can be approximated by the following Poiseuille-like expression:

$$Q = \frac{\pi R^4 \Delta P}{8 \mu_{app}(R, H_D) L}, \quad (3)$$

where  $\mu_{app}(R, H_D) = \mu_{rel} \times \mu_{plasma}$  is the apparent blood viscosity, which depends upon the local blood haematocrit, the radius of the vessel through which the blood is flowing, and the underlying plasma viscosity,  $\mu_{plasma}$  (see Eq. (5) below for a definition of  $\mu_{rel}$ ). When considering flow calculations through a network of interconnected capillary elements of distributed radii, one simply conserves mass (or flow if the fluid is incompressible) at each junction where capillary elements meet (see Fig. 2). Hence, for each node the following expression can be written

$$\sum_{k=1}^{k=N} Q_{(i,j),k} = 0, \quad (4)$$

where the index  $k$  refers to adjacent nodes and  $N = 4$  in a fully connected regular two-dimensional grid or  $N = 6$  in three dimensional. This procedure leads to a set of linear equations for the nodal pressures ( $P_i$ ) which can be solved numerically using any of a number of different algorithms (e.g. successive over-relaxation (SOR), Choleski conjugate gradient method, Lanczos method). Once nodal pressures are known, Eq. (3) can be used to calculate the flow in each capillary element in turn. A fuller discussion of the procedure can be found in McDougall et al. (2002).

### 2.2.2. Blood rheology

Blood is a very complex biphasic medium, composed of many different constituents, including: red blood cells (erythrocytes), white blood cells (leukocytes), and platelets involved in clotting cascades. These solid elements represent approximately 45% of the total blood composition in

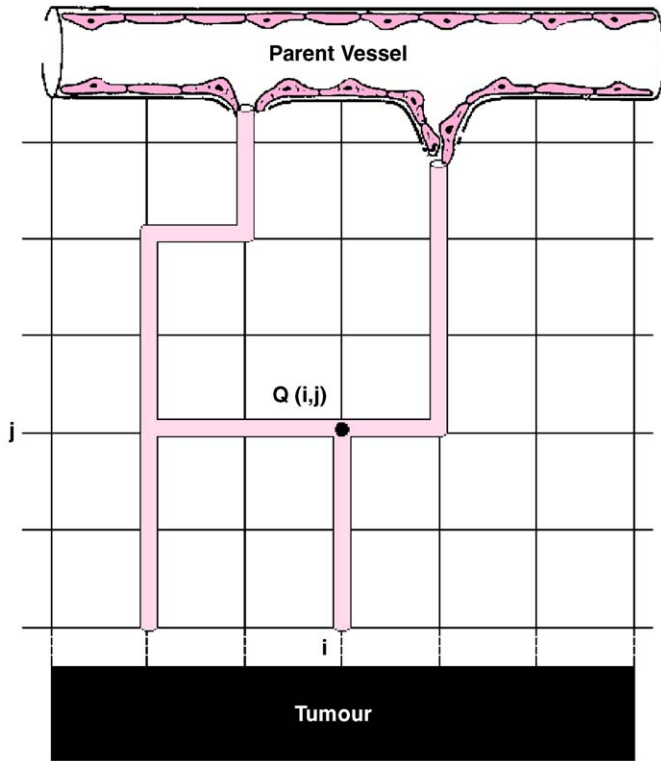


Fig. 2. Schematic representation of the capillary vessels superimposed onto the two-dimensional simulation grid used for flow calculations.

humans—red cells are predominant—and are carried in the plasma, which constitutes the fluid phase. A measure of the solid phase is given by the blood *haematocrit*, which represents the volume fraction of red blood cells contained in the blood. Hence, the average human haematocrit has a value of around 45%.

Because of its biphasic nature, blood does not behave as a continuum and the viscosity measured while flowing at different rates in microvessels is not constant. Moreover, direct measurement of blood viscosity in living microvessels is very difficult to achieve with any degree of accuracy. Pries et al. (1996) have proposed an alternative approach, which entails comparisons of the flow distribution in a numerical network (generated by a mathematical model) with similar experimental systems. The relationship which was found to offer the best fit with the experimental data at the microvascular scale, is given by

$$\mu_{rel}(R, H_D) = \left[ 1 + (\mu_{0.45} - 1)f(H_D) \left( \frac{2R}{2R - 1.1} \right)^2 \right] \times \left( \frac{2R}{2R - 1.1} \right)^2, \quad (5)$$

where  $\mu_{0.45}$  is the viscosity corresponding to the normal average value of the discharge haematocrit ( $H_D = 0.45$ ),  $R$  the vessel radius and  $f(H_D)$  a function of the haematocrit. The various terms appearing in (5) are defined

as follows:

$$\begin{aligned} \mu_{0.45} &= 6e^{-0.17R} + 3.2 - 2.44e^{-0.06(2R)^{0.645}}, \\ f(H_D) &= \frac{(1 - H_D)^C - 1}{(1 - 0.45)^C - 1}, \\ C &= (0.8 + e^{-0.15R}) \left( -1 + \frac{1}{1 + 10^{-11}(2R)^{12}} \right) \\ &\quad + \left( \frac{1}{1 + 10^{-11}(2R)^{12}} \right). \end{aligned} \quad (6)$$

Plots of Eq. (5) show that the apparent blood viscosity generally increases with decreasing capillary radius, although the precise relationship is actually haematocrit dependent. The rheological properties defined by Eqs. (5) and (6) have been used in the perfusion modelling described here.

### 2.2.3. Vessel adaptation and capillary remodelling

Blood rheological properties and microvascular network remodelling are interrelated issues, as blood flow creates stresses on the vascular wall (shear stress, pressure, tensile stress) which lead to adaptation of the vascular diameters via either vasodilatation or constriction. In turn, blood rheology (viscosity, haematocrit, etc.) is affected by the new network architecture—consequently, we should expect adaptive angiogenesis to be a highly dynamic process.

In this paper, vessel adaptation follows the treatment of Pries et al. (1995, 1998, 2001a). The model considers a number of stimuli affecting vessel diameter that account for the influence of the WSS ( $S_{wss}$ ), the intravascular pressure ( $S_p$ ), and a metabolic mechanism depending on the blood haematocrit ( $S_m$ ). These stimuli form a basic set of requirements in order to obtain stable network structures with realistic distributions of vessels diameters and flow velocities. A brief description of each now follows.

**2.2.3.1. Wall shear stress.** Many studies show that vessels adapt their radius in order to maintain a constant level of WSS (Pries et al., 1998, 2001a, b; Fung, 1993). Hence vessel radius tends to increase with increasing WSS, whilst WSS decreases with increasing radius. The WSS stimulus can be described by a logarithmic law as

$$S_{wss} = \log(\tau_w + \tau_{ref}), \quad (7)$$

where  $\tau_w$  is the actual WSS in a vessel segment calculated from

$$\tau_w = \frac{4\mu(R, H_D)}{\pi R^3} |Q| \quad (8)$$

and  $\tau_{ref}$  is a constant included to avoid singular behaviour at low shear rates (Pries et al., 2001a). Stresses in Eqs. (7) and (8) are in dynes/cm<sup>2</sup>. The WSS calculated in the parent vessel of our computational model is of the order 4 Pa (40 dynes/cm<sup>2</sup>) and capillary values are less than 2 Pa (20 dynes/cm<sup>2</sup>), in agreement with those measured experimentally in the dog by Kamiya et al. (1984). Adaptation in response to the WSS stimulus alone tends to reinforce a

single path in the network composed of a few well-established fully dilated vessels—corresponding to the main flowing “backbone” of the vasculature—whilst simultaneously eliminating the low-flow paths. However, the resulting network is “unstable” in the sense that there is no consistent balance for the radius and flow distribution achieved when  $S_{wss}$  is considered in isolation.

**2.2.3.2. Intravascular pressure.** Intravascular pressure is another key stimulus for vascular adaptation. Pries et al. (1998) have experimentally observed on the rat mesentery the dependence of the magnitude of the WSS with the local intravascular pressure ( $P$ ). They proposed a parametric description of their experimental data, which exhibits a sigmoidal increase of the WSS with increasing pressure through the following:

$$\tau_e(P) = 100 - 86 \exp\{-5000 \cdot [\log(\log P)]^{5.4}\}. \quad (9)$$

Pressure is measured in mm of mercury (1 mmHg = 133 Pa) and stresses are again given in dynes/cm<sup>2</sup>. The sensitivity of the corresponding stimulus to intravascular pressure is then described by

$$S_p = -k_p \log \tau_e(P), \quad (10)$$

where  $k_p$  is a constant that dictates the relative intensity of the stimulus.

**2.2.3.3. Metabolic haematocrit-related stimulus.** The metabolic stimulus effectively stabilizes the adapting network by stimulating vessel growth in areas of the vascular bed exhibiting low flow. The stimulus is once again described by a logarithmic law and takes the form

$$S_m = k_m \log\left(\frac{Q_{ref}}{QH_D} + 1\right), \quad (11)$$

where  $Q_{ref}$  is a reference flow. In our simulations,  $Q_{ref}$  corresponds to the flow in the parent vessel.  $H_D$  represents the discharge haematocrit in the vessels,  $Q$  the flow in the vessel under consideration and  $k_m$  is a constant characterizing the relative intensity of the metabolic stimulus.

Our theoretical model for vessel adaptation assumes that the change in a flowing vessel radius ( $\Delta R$ ) over a time step  $\Delta t$  is proportional to both the global stimulus acting on the vessel and to the initial vessel radius  $R$ , i.e.

$$\Delta R = S_{tot} R \Delta t = (S_{wss} + S_p + S_m) R \Delta t. \quad (12)$$

With the relationships described above, the model for vessel adaptation (cf. Pries et al., 1998, 2001a, b; Alarcon et al., 2003; Stéphanou et al., 2005, 2006) becomes

$$\Delta R = \left[ \underbrace{\log(\tau_w + \tau_{ref})}_{S_{wss}} - \underbrace{k_p \log \tau_e(P)}_{S_p} + \underbrace{k_m \log\left(\frac{Q_{ref}}{QH_D} + 1\right)}_{S_m} - k_s \right] R \Delta t. \quad (13)$$

The additional term  $k_s$  represents the shrinking tendency of a vessel. This term is interpreted by Pries et al. (1998) as reflecting a natural reaction of the basal lamina, which acts to counter any increase in vessel diameter.

Inclusion of the above mechanisms into our modelling framework now allows us to simulate dynamic remodelling of a flowing vasculature. This significant improvement in angiogenesis modelling allows us to describe vascular growth in a far more realistic manner, with areas of the capillary network dilating and constricting in response to variations in perfusion-related stresses and stimuli. The final step in the development of the complete DATIA model is to couple the network flow modelling approach outlined in this section to the “hollow capillary” model derived from the endothelial cell migration equations described earlier.

### 2.3. Coupling flow and cell migration through capillary branching and anastomosis

In previous models (McDougall et al., 2002; Stéphanou et al., 2005), the important mechanisms of capillary branching (the formation of new sprouts from existing sprout tips) and anastomosis (the formation of loops by fusion of two convergent capillary sprouts) followed a similar treatment to that proposed by Anderson and Chaplain (1998). Sprout branching depended only upon local TAF concentration and the impact of flow was ignored. However, this latter point can be seen as a weakness of these earlier models, as WSS is known to play a leading role in growth and branching (Pries et al., 2001a, b). In the current paper, the cell migration and flow models are coupled by incorporating the mechanism of *shear-dependent vessel branching* in addition to sprout tip branching via local TAF concentrations. Once again we quote the words of D’Arcy Thompson: “*This is a vastly important theme... and helps to bring the morphological and the physiological concepts together.*” (Thompson, 1917). In doing so, we can simulate network architectures that adapt dynamically through adjuvant vessel branching in areas of the capillary network experiencing increased shear stresses following anastomosis elsewhere in the system. We note that because the shear stress is due to the blood flowing through the capillaries, vessel branching can only occur after some degree of anastomosis has taken place—hence, the early stages of angiogenesis are characterized by TAF-dependent branching only. To summarize, the conditions for vessel branching in the new model are as follows: (i) the likelihood of a vessel branching increases with both the local TAF concentration *and* the magnitude of the shear stress affecting the vessel wall; (ii) the vessel must reach a certain level of maturation before it is able to branch, although branching cannot occur once a basal lamina has formed around a vessel (Gee et al., 2003; Benjamin et al., 1998).

## 2.4. Model parameterization and simulation details

### 2.4.1. Initial conditions

The domain considered for the computational simulation studies is a square of length  $L = 2$  mm and the parent vessel from which the vascular network grows is located at the upper edge of the domain. The tumour surface is located along the lower domain boundary. We assume that the capillary sprouts, TAF and MDE remain confined within the domain and so no-flux boundary conditions are imposed on the boundaries. Initial TAF and fibronectin profiles are the same as those used in McDougall et al. (2002), there is initially no MDE present and vascular growth is initialized by distributing five sprouts at regular intervals along the parent vessel.

### 2.4.2. Cell migration parameters

Unless otherwise indicated, the dimensionless parameter values used for the simulations presented in this paper were as follows (Anderson and Chaplain, 1998; McDougall et al., 2002; Stéphanou et al., 2005, 2006):

$$\begin{aligned} D &= 0.00035, & \delta &= 0.6, & \chi &= 0.38, & \rho &= 0.16, \\ \eta &= 0.1, & \beta &= 0.05, & \gamma &= 0.1, & \alpha &= 10e - 6, \\ \varepsilon &= 0.01, & \nu &= 3. \end{aligned}$$

Time was scaled as

$$\tilde{t} = \frac{t}{\tau}$$

with  $\tau = L^2/D_c$ , where  $L = 2$  mm was the length of the domain and  $D_c = 2.9 \times 10^{-7} \text{ cm}^2 \text{ s}^{-1}$  was taken as the diffusion coefficient for TAF (Bray, 1992). We note that the time-scale associated with the capillary growth process is of the order several days, whereas flow through the parent vessel and capillary network occurs over a time-scale of a few seconds to a few minutes. A discussion of how the two time-scales are coupled in the full adaptive model will be presented in Section 2.4.5.

### 2.4.3. Flow model parameters

In order to carry out the flow simulations, it is clear that a number of important physical and biological parameters need to be estimated.

**2.4.3.1. Vessel properties.** For the a posteriori remodelling simulations presented below, the initial radius of each capillary segment was taken to be  $6 \mu\text{m}$  and remodelling of the vessels was permitted within a range, from a minimum radius of  $2 \mu\text{m}$  (essentially eliminating flow. See Table 1) to a maximum radius of  $12 \mu\text{m}$  (see Table 1). During the DATIA simulations, nascent, non-flowing capillaries (i.e. those not yet part of the connected flowing network) were assigned  $6 \mu\text{m}$  radii and remodelling was again considered in the range  $(2, 12) \mu\text{m}$ . In all simulations, the radius of the parent vessel was kept fixed at  $14 \mu\text{m}$ . These values correspond to vessel radii at the capillary level, where the

Table 1

Typical dimension of blood cells and capillaries (after Secomb, 1995)

Dimension ( $\mu\text{m}$ )	
2	Red blood cell thickness and platelets dimension
2.8	Minimum diameter through which a red cell is able to pass
8	Red blood cell diameter
10	Mean capillary diameter
20	Size of the largest white blood cells

sizes of the vessels are very close to the size of the red blood cells (Ciofalo et al., 1999).

**2.4.3.2. Adaptation parameters.** The parameters used for the base-case adaptation model presented in Eq. (13) were taken to be

$$\begin{aligned} k_s &= 0.35, & k_p &= 0.1, & k_m &= 0.07, \\ t_{ref} &= 0.103, & Q_{ref} &= 1.909e - 11 \end{aligned}$$

(after Stéphanou et al., 2005, 2006), where  $Q_{ref}$  corresponds to the flow in the parent vessel, calculated from Eq. (3) with  $R = 14 \mu\text{m}$ ,  $L = 2$  mm and  $\Delta P = 1200$  Pa (9 mmHg) (the pressure drop across the parent vessel). The apparent viscosity  $\mu_{app}$  is calculated from Eq. (5) for each vessel segment and incorporates the effect of discharge haematocrit  $H_D$  (which is assumed to remain constant at the inlet of the parent vessel). The plasma viscosity  $\mu_{plasma}$  is  $1.2 \times 10^{-3} \text{ Pa s}$  and this parameterization gives perfusion velocities in the parent vessel of approximately  $3 \text{ mm s}^{-1}$ . The chosen parameter values pertaining to remodelling stimuli (i.e. the  $k_i$ ) yielded stable networks in all cases.

One of the main determinants of the extent of vascular remodelling is the intravascular pressure ( $P$ ). In the simulations carried out here, we have chosen inlet and outlet pressures to ensure average intravascular pressures of approximately 20 mmHg, in accordance with physiological values at the capillary scale. The effect of varying intravascular pressure will be examined in more detail later.

### 2.4.4. Tip and vessel branching probabilities

In earlier work (Anderson and Chaplain, 1998; McDougall et al., 2002; Stéphanou et al., 2005, 2006), branching at the capillary tips was assumed to depend only upon the local TAF concentration. This formulation has been used again here and the corresponding tip branching probabilities are shown in Table 2. In addition to tip branching, however, the physiologically significant process of vessel branching is also modelled as part of the current study. In order to implement this effect in the model, we assume that branching along a vessel (i.e. the generation of a new vessel which branches out at some point along an existing vessel wall as distinct from the vessel tip) depends both on the TAF concentration and on the WSS. Table 3 shows the dependence of vessel branching probability as a function of the combined effects of local WSS and local TAF

Table 2  
Sprout tip branching probabilities as a function of the local TAF concentration

TAF concentration	Sprout tip branching probability
$\leq 0.3$	0.0
]0.3–0.5]	0.2
]0.5–0.7]	0.3
]0.7–0.8]	0.4
$> 0.8$	1.0

Table 3  
Vessel branching probabilities as functions of the local TAF concentration and the magnitude of the local wall shear stress

[TAF]/TAF <sub>max</sub>	WSS/ $\tau_{max}$				
	[0.0,0.2[	[0.2,0.4[	[0.4,0.6[	[0.6,0.8[	[0.8,1.0]
[0.0,0.3[	0.00	0.00	0.00	0.00	0.00
[0.3,0.5]	0.00	0.02	0.04	0.06	0.08
[0.5,0.7[	0.00	0.03	0.06	0.09	0.12
[0.7,0.8[	0.00	0.04	0.08	0.12	0.16
[0.8,1.0]	0.00	0.10	0.20	0.30	0.40

TAF<sub>max</sub> is the maximum TAF concentration at  $t = 0$  and  $\tau_{max} = 2$  Pa (20 dynes/cm<sup>2</sup>), the maximum shear stress derived from preliminary flow simulations.

concentration. In the absence of quantitative experimental data, the probabilities chosen for the vessel branching process have been defined on a qualitative basis and reflect the combined influence of the WSS and local TAF concentration. High values of WSS in tandem with high local TAF concentrations lead to a higher branching probability at that point in the vessel wall, whilst lower values of one or both of WSS and TAF concentration lead to a lower branching probability. For each range of WSS (linearly distributed in [0,1]), the corresponding TAF probability profile has been obtained via a linear scaling of the values reported in McDougall et al (2002) and Stéphanou et al. (2005, 2006). Note that in the absence of WSS, TAF-dependent sprout tip branching is the only means by which a migrating vessel can bifurcate.

One additional constraint on vessel branching is the age of the vessel itself. The time interval within which a vessel can branch has been fixed at [4–8] days in the simulations (i.e. from  $\tilde{\tau} = 2.66$  to 5.33). In this interval, the vessel is sufficiently mature for branching to occur yet young enough to ensure that no basal lamina has had time to form (which would contribute considerably to the stabilization of the network; Benjamin et al., 1998; Morikawa et al., 2002).

#### 2.4.5. Coupling growth and flow time-scales

As mentioned earlier, the time-scales associated with the endothelial cell migration and the flow processes are vastly

different—formation of the tumour-induced vasculature occurs over the course of several days, whilst the parent vessel/capillary network can be completely perfused within minutes.

In order to address this issue without compromising computational efficiency, it became necessary to develop a simulation framework that allowed remodelling to occur during the growth phase. An idealized procedure is as follows: (i) model the growth of the capillary network on a time-scale  $\tilde{\tau}$ , using the endothelial cell migration model; (ii) pause the endothelial cell migration model whenever a new anastomosis (loop) forms; (iii) switch time-scales and flow/remodel the entire capillary network using Eqs. (3)–(6) and (13) as a result of the modified flow geometry until a new steady state has been reached (this typically takes  $\sim 100$  s); (iv) resume network growth using the cell migration model on the  $\tilde{\tau}$  time-scale.

During the later stages of a simulation, however, the number of anastomoses (loops) increases considerably and the above procedure becomes impractical from a computational point of view. Consequently, it was decided to flow the network to steady state at regular intervals during the growth process. A sensitivity study showed that remodelling at intervals of  $\Delta\tilde{\tau} = 4.0$  was sufficient to produce vascular networks consistent with those generated from simulations incorporating more frequent adaptation.

Returning to the time-scale for flow, it should be noted that the time-step required when dealing with calculations involving convective transport within a network must be less than or equal to the minimum time required for the least efficient capillary element in the network to empty; i.e.  $\Delta t = \text{MIN}(V_{cap}/Q_{cap})$ , where  $V_{cap}$  and  $Q_{cap}$  correspond to the volume and flowrate of a capillary element. This procedure ensures that mass (in this case erythrocyte mass through haematocrit) is conserved during a simulation.

### 3. Simulation results

Results are presented in the following section corresponding to a number of different stages in the formulation of the full DATIA model. The section begins with a simulation demonstrating the effect of explicitly incorporating MDE activity into the endothelial migration model. At this stage, no flow/remodelling is considered and only sprout branching at the vessel tips has been allowed (i.e. there is no vessel branching due to WSS). The main point of interest in this first set of computational simulations is to assess the effect of MDEs upon endothelial cell migration. Subsequent results incorporating flow will show the impact of dynamic remodelling and shear-induced vessel branching upon the global network architecture. Finally, once the full DATIA model is implemented, a number of key physical and biochemical parameters are varied in the model to assess their effect upon treatment delivery to the tumour—these results highlight a number of new therapeutic targets for tumour management.

### 3.1. Capillary network architecture in the absence of flow

The model for tumour-induced capillary growth described by the system of Eqs. (1) and (2) was solved numerically on a  $100 \times 100$  ( $x, y$ ) square grid. The system of Eq. (2) was solved for each grid point at each time step and the resulting variables  $c$  and  $f$  were then used to calculate the coefficients  $P_0$ – $P_4$  appearing in the discretized form of Eq. (1). These coefficients were then used to calculate the migratory direction of each endothelial cell at the vessel tip at each time step of the simulation, i.e. the direction of growth of each sprout.

Figs. 3 and 4 present the simulation results associated with an initial linear gradient of TAF—Fig. 3 shows the network growth and vascular architecture, whilst Fig. 4 shows the associated MDE concentration in the ECM. We observe in Fig. 3 the stochastic nature of each of the five sprout trajectories as they progress towards the tumour (the surface of which occupies the lower boundary of the domain). Initially, the MDE concentrations are highly localized around the individual sprout tips and the migratory path taken by each vessel is essentially independent of its neighbours. At time  $\tilde{\tau} = 2.6$  (corresponding to  $t = 3.9$  days), vessels 2 and 3 (numbered from left to right) begin to converge and by  $\tilde{\tau} = 5.2$  (7.8 days) some degree of sprout branching and local anastomosis has already taken place for all five sprouts. Vessels 2 and 3 have now formed an anastomosis (loop)—hence perfusion could be expected to occur within the developing capillary bed at this time (as will be described later when discussing the full DATIA model).

Anastomosis increases considerably with increased sprout branching in regions distal to the parent vessel and the individual vascular trees rapidly connect with one another after  $\tilde{\tau} = 6$  (9 days). Regions of high MDE concentration subsequently emerge as the number of migrating, productive tip cells rises and it becomes clear that the increase in anastomosis is related to an increase in lateral migration due to the appearance of a connected MDE front as shown in Fig. 4 (from  $\tilde{\tau} = 6$ ). It takes approximately 10 days for the growth process to be completed, i.e. for the vasculature to connect the tumour to the parent vessel and hence to the blood supply.

The vascular architectures produced by the model at this stage are in good agreement with experimental data (Gimbrone et al., 1974; Muthukkaruppan et al., 1982) but the resulting vascular networks lack any variation in capillary radius (a vital factor when considering treatment efficacy). Moreover, vessel branching at this stage only depends upon the local TAF concentration and is unaffected by perfusion. The following sections present results that address these issues, together with an examination of the roles played by a number of important physical and biochemical parameters.

### 3.2. *A posteriori* remodelling of a pre-formed vasculature network

The first step towards the development of a full DATIA involves the temporal variation of capillary radii. In this section, attention is focussed upon vessel adaptation in the context of an already fully formed, flowing vascular

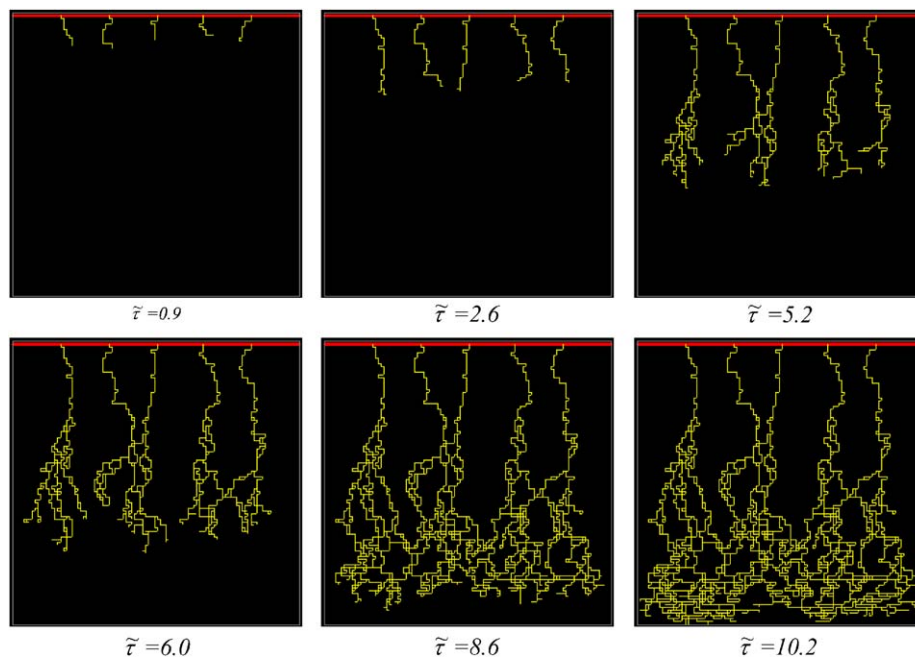


Fig. 3. Spatiotemporal evolution of a developing hollow capillary network. The figure shows the migration of the ECs at the vessel tips and the paths they follow as they migrate through the ECM in response to TAF gradients (chemotaxis) and FN gradients (haptotaxis). The paths of the tip cells define the subsequent vessel structure. Tip branching and vessel fusion (loop formation or anastomosis) are also included in the model.

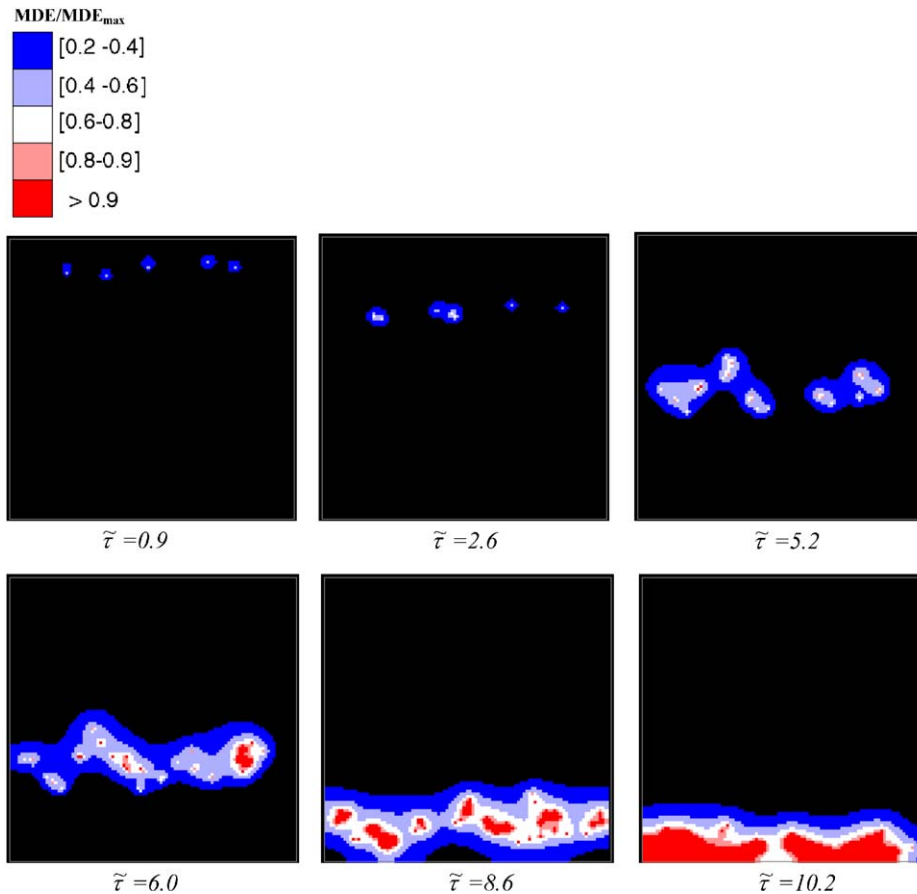


Fig. 4. Spatiotemporal evolution of the MDE concentration in the ECM associated with the developing capillary network shown in Fig. 3. The MDE concentration is largely localized at the sprout tips (where it is produced by the ECs) but slowly diffuses into the ECM as time progress.

network. Initially, the capillary vessels are considered to be devoid of red blood cells and a constant input haematocrit of 45% is set at the inlet end of the parent vessel. Vessel radii then dilate/constrict in accordance with Eq. (13).

Note that Eq. (13) includes terms involving shear stress, flow, and intravascular pressure, the first two of which also depend upon haematocrit, relative viscosity and capillary radius through Eqs. (5) and (6). Consequently, an increase in haematocrit into a capillary element leads to an increase in relative viscosity, which in turn affects the flow through that element (assuming, for the moment, that the pressure drop across that element remains unchanged). Hence, it may be concluded that it is the  $\mu_{rel}(R, H_D)$  relationship from Eq. (5) that primarily dictates the magnitude of the haematocrit-related stimulus  $S_m$ . While this argument is broadly correct, the fact that the vessel radii are changing temporally means that the overall picture is somewhat more complex. Intravascular pressure does *not* remain unchanged within a capillary element during a simulation—as radii dilate and constrict, the pressure field throughout the capillary network must be recalculated after each time step and the new pressure values used in the recalculation of all three dynamic stimuli. Hence, radial perturbations, vessel haematocrit, relative viscosity, intravascular pressure, WSS and capillary flow are all inter-

related and interact in a rather complex nonlinear way in the context of network calculations.

Fig. 5 shows the evolution of a pre-formed vascular network under the influence of perfusion. Initially, all vessel radii (except those of the parent vessel) were set at  $6\ \mu\text{m}$  and the simulation was run until a steady state had been reached (at approximately  $t = 300\ \text{s}$ ). Once erythrocytes begin to enter the system from the parent vessel inlet, the capillaries begin to dilate or constrict within the bed according to Eq. (13). At  $t = 0.8$ , it can be seen that vessels 1 and 5 have dilated to the greatest extent. This is due to the fact that topologically these vessels essentially constitute the main inlet and outlet pathways to and from the parent vessel and consequently remove and return the majority of the haematocrit. A fully dilated loop first emerges at  $t = 2.4$  with a second extensive dilation beginning at the same time in the loop composed of vessels 2 and 3.

Subsequent remodelling is accompanied by fluctuations in the network architecture, with some regions of the vasculature undergoing successive cycles of dilation and constriction. This is clearly evidenced in the later snapshots in Fig. 5, where a centrally located vessel is dilated at  $t = 4.5$ , substantially constricted at  $t = 72$ , and further dilated by  $t = 295$ . Whilst this particular fluctuation is

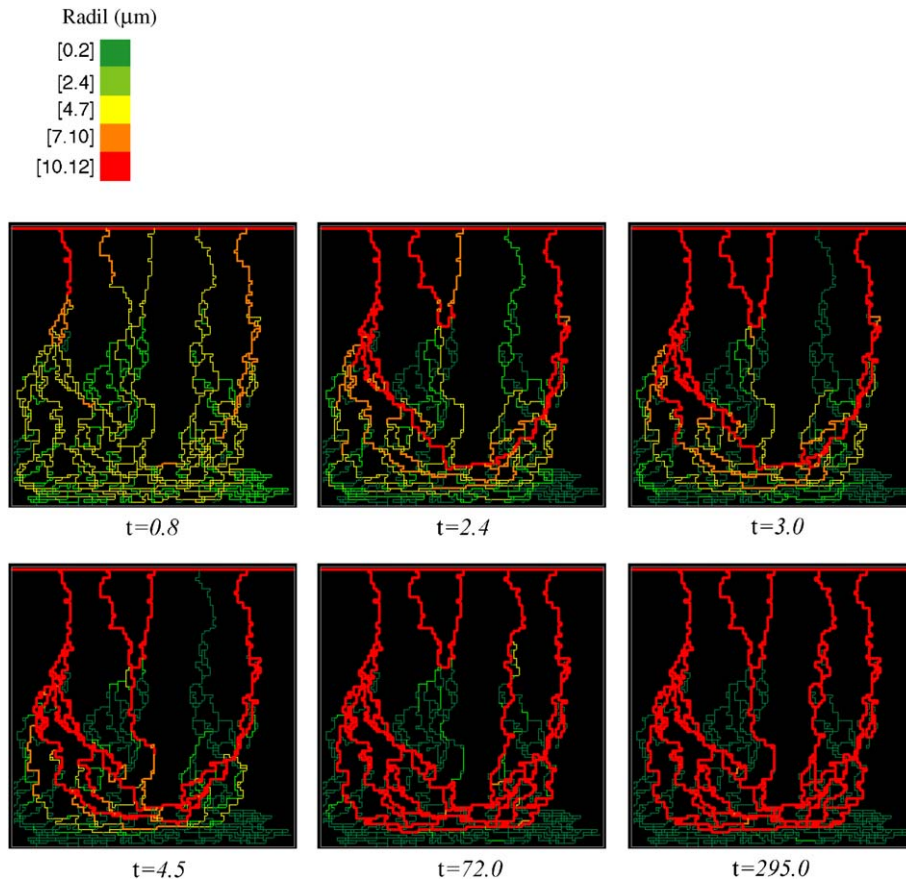


Fig. 5. Snapshots showing the a posteriori remodelling of a hollow capillary network. The figures show the evolution of several fully dilated vessels containing most of the flow. These vessels form the “backbone” of the remodelled network. Note that the time values reported in Fig. 5 are in seconds and are not dimensionless (dimensionless time  $\tilde{\tau}$  is used in this paper when discussing capillary growth, see Section 2.4.5).

mainly due to the fact that the central vessel lies close to the boundary between efferent and afferent capillaries, a similar phenomenon occurs within the highly connected regions of the network.

After approximately 300 s, the network reaches steady state and no further remodelling occurs. It can be seen that, for a given pre-defined “hollow” network architecture generated from the endothelial cell migration model, remodelling due to perfusion results in the development of several well-defined fully dilated vessels carrying almost all the flow. As will be demonstrated later, it is the structure of these fully dilated flowing vessels which determines the efficacy of both nutrient delivery to the tumour and any therapeutic treatment that may subsequently be applied.

### 3.3. DATIA without shear-induced branching

The next stage in the model development is to consider vessel adaptation during growth. This is achieved using the procedure outlined in Section 2.4.5, whereby the developing network is flowed at regular intervals until a steady state is obtained. The case presented in this section does not include shear-induced vessel branching. Snapshots from the base-case perfusion simulation are shown in Fig. 6 on a time-scale of the dimensionless time variable  $\tilde{\tau}$ .

At  $\tilde{\tau} = 2.6$ , it can be seen that the five initial sprouts have migrated towards the tumour surface, although no anastomoses have yet occurred. Consequently, no flow is possible in the capillary network at this stage and the vessels begin to constrict—only the tips of the migrating capillaries have radii greater than the minimum value, as these are the most recently formed vessel segments and are assigned a default radius of  $6 \mu\text{m}$  upon formation.

The first anastomosis (closed loop) is formed at time  $\tilde{\tau} = 4.0$  (6 days) by the fusing of vessels 2 and 3 (numbered from left to right). As noted in Section 2.4.5, the time-scale for the flow processes is much shorter than for the cell migration. At this stage in the simulation, flow through this loop and its effect on the network was considered using Eqs. (3)–(6) and (13) until a new steady state was reached. As noted in Section 2.4.5, this process typically takes  $\sim 100$  s. Consequently, the development of this loop is shown in Fig. 6 at times  $\tilde{\tau} = 4.0$ ,  $\tilde{\tau} = 4.0 + \varepsilon_1$ , and  $\tilde{\tau} = 4.0 + \varepsilon_1 + \varepsilon_2$ , where the  $\varepsilon_i$  are “small” times of the order 100 s. Endothelial cell migration and vessel formation continue with additional TAF-induced sprout branching and anastomosis. At  $\tilde{\tau} = 12.0$  (approximately 18 days), all five primary vessels have branched and connected to form a fully connected capillary network that reaches the tumour surface. Subsequent perfusion of this structure leads to the

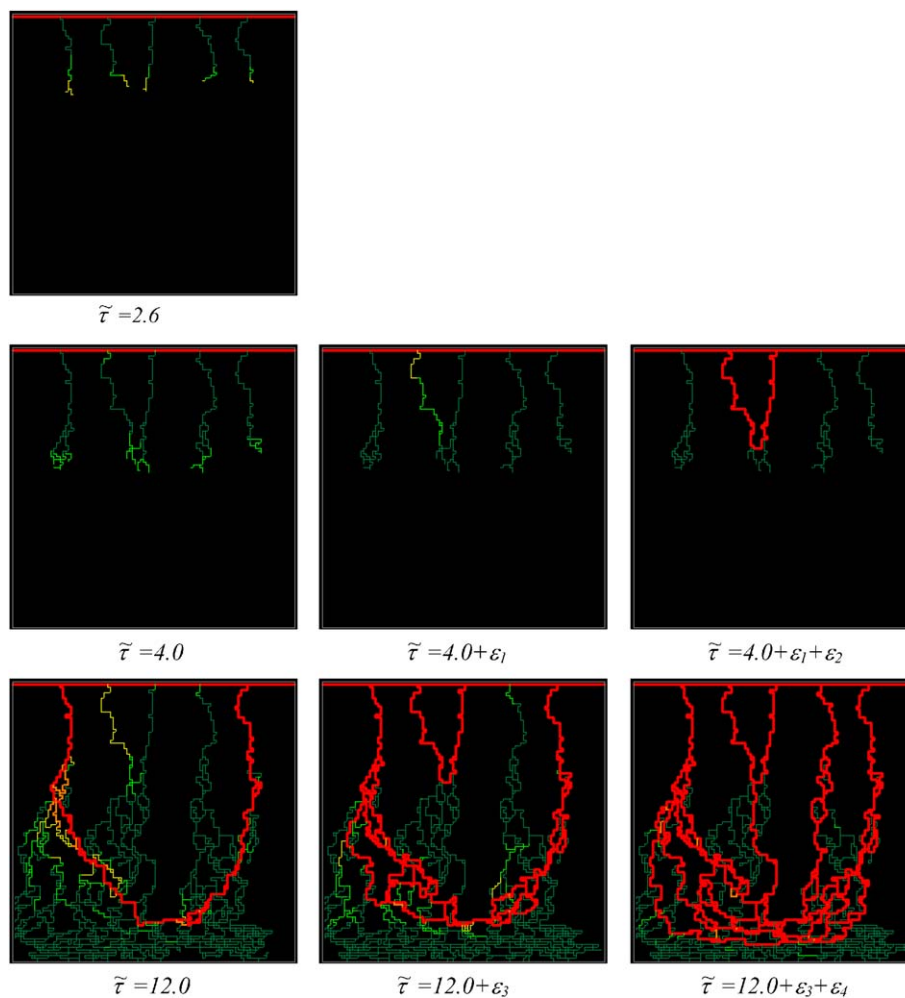


Fig. 6. Snapshots showing the evolution of a capillary network undergoing remodelling during growth but with no shear-induced branching. The  $\varepsilon_i$  are times of the order of 100 s, which is the typical flow-rate time-scale (see Section 2.4.5 for details). The final steady-state network structure is the same as that in Fig. 5 because there is no coupling of the flow to the growth through shear-induced branching.

formation of a larger-scale loop which dilates, draws additional haematocrit from the parent vessel, and begins to feed neighbouring capillaries. The final steady-state vasculature is shown in Fig. 6 at time  $\tilde{\tau} = 12.0 + \varepsilon_3 + \varepsilon_4$ . In fact, the final network architecture and distribution of capillary radii are identical to those obtained from the a posteriori remodelling simulation. This is because the migration and flow models are essentially uncoupled at this stage of the model development—although the topology of the network does affect the spatial distribution of flow and hence the spatial distribution of vessel radii, the flow itself does not affect the subsequent migration of capillary sprouts. The coupling of migration and flow occurs through the inclusion of *shear-induced vessel branching* and this will be considered next.

### 3.4. DATIA including shear-induced branching

In the simulation results of the previous section, only *capillary sprout tip* branching was considered. The series of simulations reported in this and subsequent sections,

however, includes both sprout tip branching and *vessel branching* under the combined effects of both local TAF concentration and additionally *local wall shear stress*. This crucial effect is one aspect of the current model that has not been modelled in previous work.

For the sake of brevity, some of the intermediate snapshots of developing capillary beds have had to be omitted and only the final architectures ( $\tilde{\tau} = 30.0$ ) are presented in some cases (collated later in Fig. 9). This has the additional benefit of facilitating direct comparisons to be made between vasculatures as model parameters are varied. The resulting vascular structures can be compared with that generated without shear stress branching discussed in Section 3.3. Note that sprout tip branching is still important in the production of the first connections between the growing vascular trees, allowing blood to flow into the evolving capillary bed and creating the shear stresses required for the additional vessel branching.

Clearly, the early vessel development must be identical to that observed earlier up to the point where the first loop forms at  $\tilde{\tau} = 4.0$ —vessel branching only begins after the

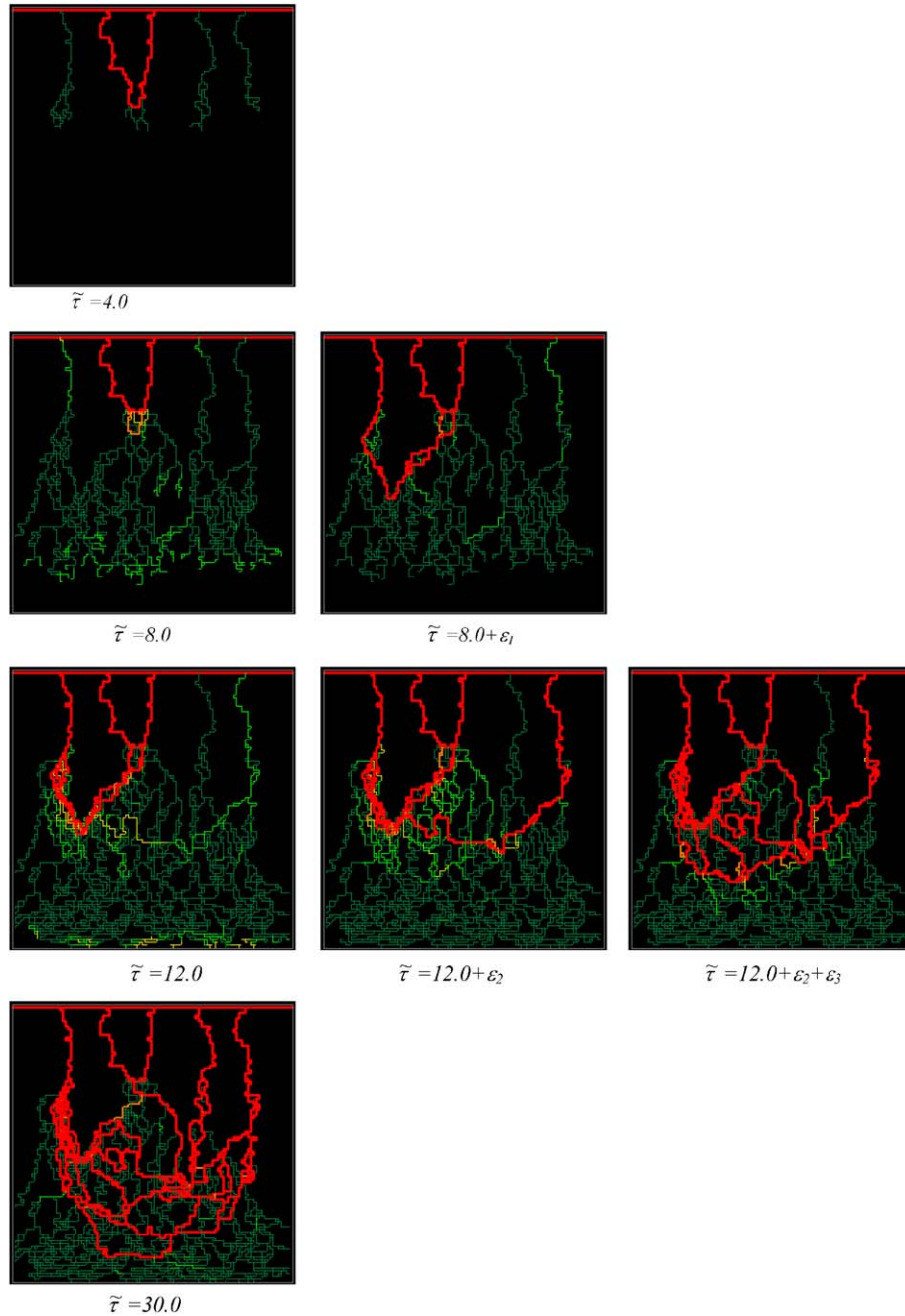


Fig. 7. Snapshots showing the evolution of a capillary network using the full DATIA model, including shear-stress-induced branching. The  $\epsilon_i$  are times of the order of 100 s, which is the typical flow-rate time-scale (see Section 2.4.5 for details). Both the transient and final steady-state network structure is radically different from that of Figs. 5 and 6 indicating the importance of coupling flow effects to network growth.

vascular networks contains connected loops, as only then can capillaries become perfused with blood and shear stresses exerted on vessel walls. Fig. 7, depicting the full DATIA simulation including shear-induced branching, confirms this.

The network architecture at later times, however, diverges considerably from that shown in Fig. 6. After  $\tilde{\tau} = 4.0$ , additional shear-induced branches emerge from the apex of the loop formed by the anastomosis of vessels 2 and 3. These branches continue to migrate towards the tumour ( $\tilde{\tau} = 8.0$ ) and modify the distribution of flow and

wall shear-stress at subsequent times. Further shear-induced branching is evident in the snapshots at  $\tilde{\tau} = 12.0$  (18 days), largely associated with the dilated arcade between vessels 1 and 2. The network is essentially at steady state at this stage, with only a small amount of vessel branching occurring after this time.

The most important aspect of this simulation is that it demonstrates how shear-induced branching leads to earlier formation of dilated anastomoses close to the parent vessel. This dilation is positively reinforcing, with proximally dilated loops undergoing further vessel branching.

Subsequent migration of these additional branches results in high capillary densities and the main consequence of this is that the number of dilated, high conductivity pathways close to the tumour surface is greatly reduced. The impact of these changes in network architecture upon treatment delivery will be discussed later in Section 4.

### 3.5. DATIA—sensitivity to wall shear stress

The results presented in this section examine the sensitivity of the vessel branching process to WSS. This is achieved by reducing the branching requirements in terms of  $\tau_{max}$ , the maximum WSS measured in the base-case simulation presented in Section 3.4.

Fig. 8 shows the capillary network development when the critical value is reduced to  $\tau_{max} = 1.0$  Pa (representing a 50% reduction in the base-case value of  $\tau_{max} = 2.0$  Pa). An increased amount of branching activity is observed at the apex of the loop formed by vessels 2 and 3 in comparison to the previous DATIA simulation and the shear-induced branching occurs earlier (at  $\tilde{\tau} = 7.5$ ). A double loop of dilated capillaries forms at  $\tilde{\tau} = 8.0$  and this is soon followed by a burst of vessel branching and a consequent increase in local vessel density all around the loop. Further bursts of branching are observed around the main structure, with neighbouring vessel segments dilating and reinforcing what is, to all intents and purposes, a capillary shunt.

These results clearly show that the sensitivity of the developing vasculature to WSS is an important determinant of capillary network topology. Moreover, manipulation of the degree of sensitivity could prove to be an

important therapeutic target—for example, vasculatures such as those shown in Fig. 8 would be poorly suited to supplying nutrients to a developing tumour and so any therapy that increased capillary branching could prove beneficial in starving the tumour. However, it should also be noted that any chemotherapy treatment aimed at targeting tumour cells and injected upstream of such a network would yield poor treatment efficacy—the highly dilated shunt would effectively remove any drug from the system before it had time to reach the tumour.

The first two pictures from the collated results (Figs. 9a and b) show the vascular structures resulting from additional simulations examining the vessel branching issue. In Fig. 9a, the vessel branching probabilities were smaller than those presented in Table 3 by a factor of 2.5, whilst in Fig. 9b the branching probabilities were smaller by a factor of 5 ( $\tau_{max} = 1.0$  to facilitate comparisons with Fig. 8). As expected, a reduction in sensitivity to WSS reduces the overall capillary density and this ultimately leads to the formation of a dilated flowing backbone that is far less compact than before. The capillary shunt observed earlier is now replaced by a more dendritic vascular architecture.

Given the above discussion and the results shown in Figs. 8, 9a and b, it is evident that additional experimental research would be highly desirable to help elucidate and quantify the mechanisms whereby shear-induced branching occurs; the chemical mediators involved, the role played by convective transport, and the sensitivity of ECs to the associated signalling molecules. The implications for therapeutic intervention could then be more fully evaluated.

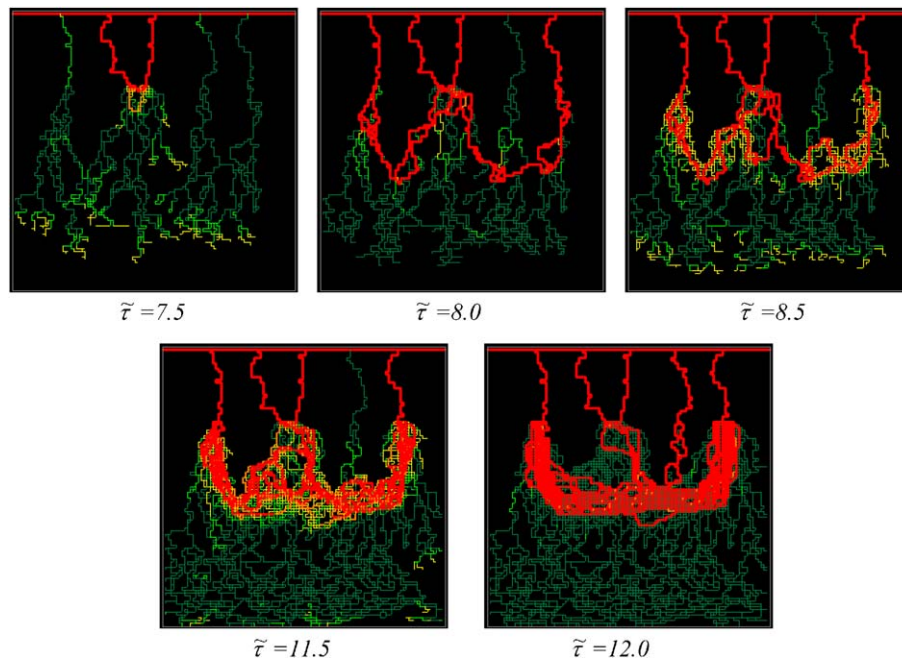


Fig. 8. Snapshots showing the development of a capillary network structure with a reduced WSS parameter  $\tau_{max} = 1.0$  Pa. The results of the simulation show the development of what is essentially a capillary shunt with no flow reaching the lower boundary.

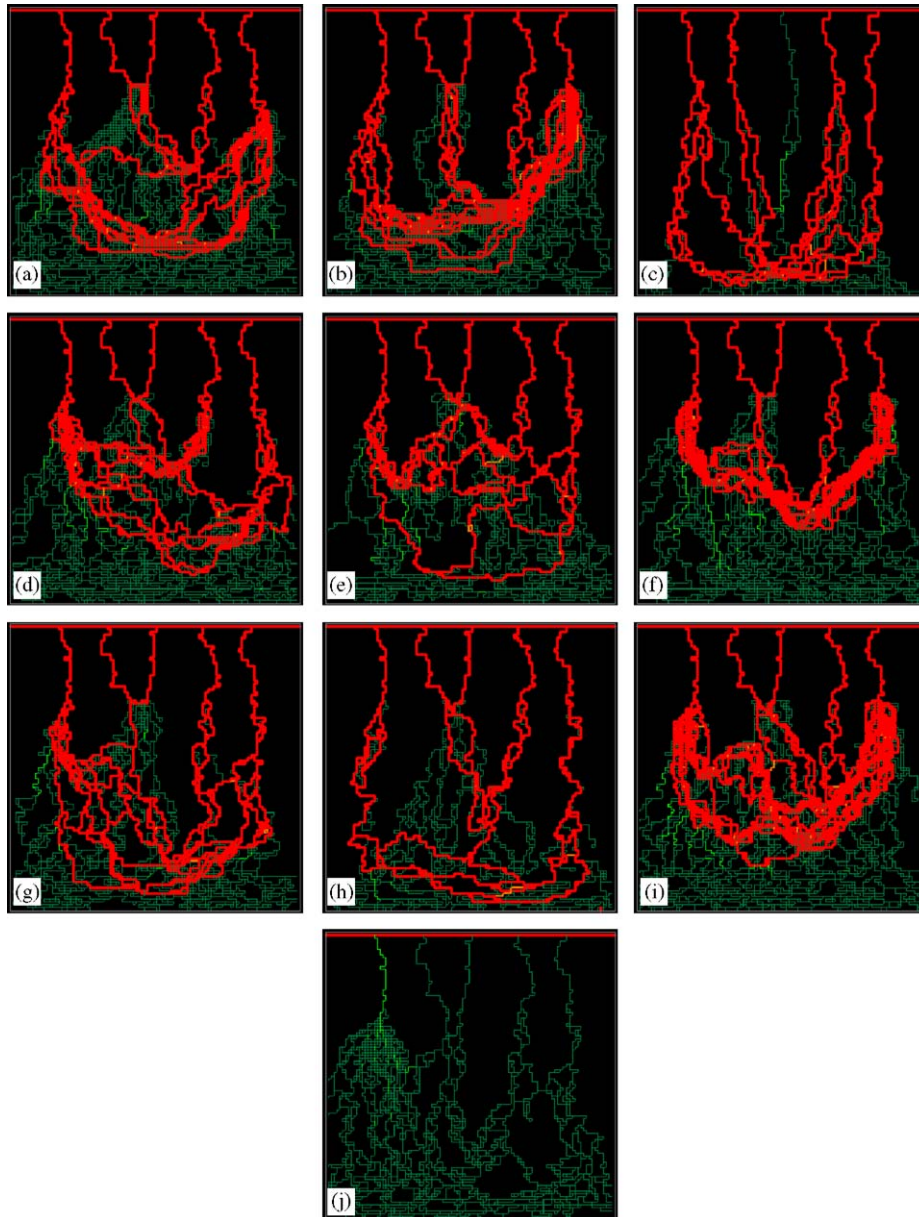


Fig. 9. Plots showing the different steady-state capillary network structures which have evolved after a dimensionless time  $\bar{\tau} = 30$  due to changes in model parameters. (a) reduced WSS parameter  $\tau_{max} = 1.0$  Pa and branching probabilities reduced by a factor of 2.5; (b) reduced WSS parameter  $\tau_{max} = 1.0$  Pa and branching probabilities reduced by a factor of 5; (c) reduced haptotactic coefficient  $\rho = 0.16$ ; (d) increased plasma viscosity  $\mu_{plasma} = 4.8 \times 10^{-3}$  Pa s; (e) increased input haematocrit  $H_D = 0.675$ ; (f) reduced input haematocrit  $H_D = 0.225$ ; (g) increased inlet and outlet blood pressure ( $P_{in} = 2960$  Pa,  $P_{out} = 1760$  Pa); (h) reduced inlet blood pressure ( $P_{in} = 2960$  Pa,  $P_{out} = 2060$  Pa); (i) reduced outlet blood pressure ( $P_{in} = 3260$  Pa,  $P_{out} = 1760$  Pa); (j) increased vessel sensitivity to intravascular pressure ( $k_p = 0.5$ ).

### 3.6. DATIA—sensitivity to haptotaxis parameter

The migratory direction of any given endothelial cell from the parent vessel to the tumour surface is affected by a number of parameters that incorporate the effects of random, chemotactic and haptotactic movement (cf. Eq. (1)). In this section, computational simulation results are presented that examine the differences in the capillary network architecture when the haptotactic coefficient  $\rho$  is varied. Whilst all previous simulations to this point have used a value of  $\rho = 0.28$ , Fig. 9c shows the vasculature

which develops when  $\rho = 0.16$ , i.e. when the strength of the haptotactic response has been reduced. All other parameters were the same as those used in Section 3.4.

In contrast to the simulations where  $\rho = 0.28$ , the capillary vessels are found to grow towards the tumour surface in a more directed fashion and lateral migration is reduced. This is not unexpected given the endothelial cell chemotactic response to TAF and is also in line with the results of Anderson and Chaplain (1998). One major consequence of this more directed vessel growth is the delay in the formation of anastomoses and subsequent

perfusion from the parent vessel. In the simulation, a small amount of perfusion only begins at  $\tilde{\tau} = 6.7$  (approximately 10 days, not shown), compared with  $\tilde{\tau} = 4.0$  (6 days) when  $\rho = 0.28$ . Even at this time, however, the network structure is such that capillary flows are very low and vessel remodelling is minimal. Only at times in excess of  $\tilde{\tau} = 12.0$  do vessels dilate appreciably and give rise to wall shear stresses of sufficient magnitude to cause vessel branching. A small amount of shear-induced branching emerges at  $\tilde{\tau} = 16.0$  and  $30.0$  but these new capillaries merely penetrate small, insignificant islands of un-vascularized tissue and do not perturb the existing flowing backbone.

These results not only highlight the important role played by cell–matrix interactions during angiogenesis, but also emphasize the way in which several apparently unconnected phenomena can interact throughout the process. Although the only direct coupling between perfusion and cell migration in the model is that related to shear-induced branching, the distribution of intravascular pressure and flow is actually affected by the local network architecture, which is, in turn, effectively controlled by the underlying cell biology (through chemotaxis and haptotaxis). Hence, not only does perfusion modify the network topology (through vessel branching), but the evolving topology itself affects the subsequent distribution of shear stresses and new branches—another link is established between perfusion, capillary remodelling, and the biological processes.

### 3.7. DATIA—sensitivity to blood properties

Having examined the effects on the network structures of varying a number of parameters related primarily to the ECs forming the capillaries, we next turn attention to the properties of the blood itself. The first parameter sensitivity examines the impact of increasing the viscosity of the plasma ( $\mu_{\text{plasma}}$ ) entering the system through the parent vessel. We note that this effectively increases the apparent viscosity used in determining vessel flow through Eq. (3). A plasma viscosity four times greater than that used in all other simulations was considered (i.e.  $\mu_{\text{plasma}} = 4.8 \times 10^{-3}$  Pa s here). All other parameters were the same as those used for the simulations presented in Section 3.4.

The structure of the capillary network generated is shown in Fig. 9d and is seen to be similar to that obtained using a plasma viscosity of  $1.2 \times 10^{-3}$  Pa s (cf. Fig. 7). Intuitively, one might expect higher viscosities to yield higher wall shear stresses (and hence increased vessel branching) through Eq. (8), but this assumes an increase in viscosity without a concurrent change in vessel flow. This is not the case here, however, as fixed inlet and outlet pressure boundary conditions are used (these will be varied later). Consequently, any increase in blood viscosity will cause a decrease in capillary flow everywhere in the network and the WSS will actually remain unaffected. This is clear from Eq. (8) in the context of a single capillary tube—in this case, the WSS is given by  $\tau_w = (r\Delta P)/(2L)$

(i.e. the WSS is independent of viscosity), where  $r$  is the capillary radius,  $\Delta P$  the associated pressure drop and  $L$  the tube length. It can therefore be concluded that modifying plasma viscosity will not appreciably affect the final network structure.

Whilst the effect of changing the plasma viscosity is unproblematic to interpret, the impact upon network structure of varying the input haematocrit is less straightforward to predict. This is due to the fact that a number of controlling variables (radial perturbations, relative viscosity, intravascular pressure, WSS and capillary flow) are affected by variations in haematocrit simultaneously. Consequently, their individual contributions are difficult to isolate in the context of flow through interconnected networks.

As discussed earlier in Section 3.2, an increase in haematocrit locally into a capillary element results in an increase in relative viscosity, which decreases the flow through that element. However, unlike the viscosity sensitivity discussed above, where  $\mu_{\text{plasma}}$  was increased uniformly throughout the system, the haematocrit varies both spatially and temporally. Hence, there is no way of predicting a priori what effect changing the input haematocrit may have upon the developing vasculature because of the nonlinearities associated with this parameter (although it is clear that the  $\mu_{\text{rel}}(R, H_D)$  relationship in Eq. (5) plays a major role).

In order to address this issue, two simulations were carried out at different input haematocrits:  $H_D = 0.675$  and  $0.225$ . These values represent a 50% increase and decrease in the perfusion base-case value of  $0.45$ , respectively. Fig. 9e shows the results for  $H_D = 0.675$  at time  $\tilde{\tau} = 30.0$ . Although some minor perturbations are apparent, the overall network architecture is similar to that found earlier in Fig. 7, Section 3.4, and it appears that increasing input haematocrit above the physiological norm will have very little effect upon tumour-induced angiogenesis (and hence upon the supply of nutrients and/or treatments to the tumour). This is not the case, however, if the haematocrit is reduced below the physiological norm.

Capillary network growth with  $H_D = 0.225$  is shown in Fig. 10 (final configuration is reproduced in Fig. 9f) and this simulation highlights some interesting features of dynamic adaptive angiogenesis. Initially, there appears to be less vessel branching than was observed in the simulation reported in Fig. 7, Section 3.4—in fact, at  $\tilde{\tau} = 4.0$  the capillaries have dilated to a far lesser degree and the primary loop formed from vessels 2 and 3 is poorly developed. After a time  $\tilde{\tau} > 8.0$ , however, the distribution of haematocrit is such that a burst of vessel branching occurs around the developing larger transverse loop (essentially connecting the original vessels 1 and 5): vessel density around the loop continues to increase and the high-flow bypass becomes further reinforced. Although initial differences in global topology are small when compared to the network generated in Fig. 7, it is evident that such small

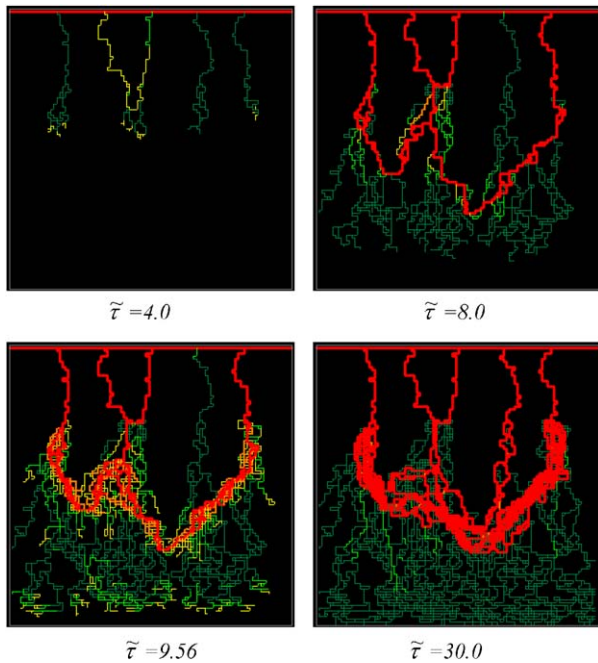


Fig. 10. Snapshots showing the development of a capillary network formation where the blood has a reduced input haematocrit of 0.225.

variations can have a dramatic impact upon angiogenesis when coupled with local variations in vessel haematocrit. The hypothesis here is that a reduction in input haematocrit during angiogenesis could lead to the formation of highly dilated loops close to the parent vessel. The therapeutic implications of this will be explored further in Section 4.

### 3.8. DATIA—pressure sensitivities

The final set of parameter sensitivities presented in this paper examines the related issues of intravascular pressure and the pressure drop across the parent vessel feeding the developing capillary network. The results presented so far have assumed fixed inlet and outlet pressures of 3260 Pa (24.5 mmHg) and 2060 Pa (15.5 mmHg), respectively. Consequently, intravascular pressures calculated within the capillary network proximal to the parent vessel are distributed around 2660 Pa (20 mmHg), whilst pressures in distal regions (i.e. close to the tumour surface) remain somewhat lower. Note that, (i) the *magnitudes* of these intravascular pressures help determine the degree of vessel constriction through Eqs. (10) and (13), and (ii) *gradients* in intravascular pressure determine flow. Therefore both vessel constriction and flow in the network are affected by changes in the inlet and/or outlet pressure associated with the parent vessel.

We first examine the impact of varying the intravascular pressure profile upon network development by decreasing both the inlet and outlet pressures by 300 Pa (2.25 mmHg). The final vasculature (at  $\tilde{\tau} = 30.0$ ) is shown in Fig. 9g and is similar to that found in the perfusion base-case of Fig. 7,

Section 3.4. This is as expected because the pressure *gradients* are identical to those calculated earlier—only the magnitudes of the intravascular pressures have changed (now distributed around 2360 Pa (17.75 mmHg)) and these changes have not been sufficient to substantially affect radial adaptations through Eq. (13).

Next, the inlet blood pressure was decreased to 2960 Pa (22.25 mmHg), whilst the outlet pressure remained fixed at 2060 Pa (15.5 mmHg). In this case, all capillary flows are reduced due to the decrease in the global pressure drop, vessel branching diminishes and the resulting dilated backbone is less dense than before (Fig. 9h). In fact, the final network architecture is closer to that obtained by reducing the haptotactic coefficient (cf. Fig. 9c). This again emphasizes the way in which perfusion can affect the interpretation of the underlying biological processes in an unexpected manner.

The final sensitivity to intravascular pressure gradients involved decreasing blood pressure at the outlet of the parent vessel by 300 Pa (2.25 mmHg), whilst keeping the inlet pressure fixed at 3260 Pa (24.5 mmHg). In this case, pressure gradients are the largest considered so far and an increase in the density of shear-induced branching is observed (Fig. 9i, note that there is an increased number of new sprouts close to the apex of the loop formed by vessels 2 and 3). The heavily dilated anastomoses are reminiscent of those obtained when the haematocrit was decreased or the sensitivity of ECs to shear-induced branching was increased.

Having examined the role played by pressure boundary conditions at the parent vessel, attention is next focussed upon the role played by intravascular pressure during radial adaptation. For this final simulation, fixed inlet and outlet pressures of 3260 Pa (24.5 mmHg) and 2060 Pa (15.5 mmHg) were used once again but the sensitivity of the capillaries to the intravascular pressure stimulus (see Eqs. (9) and (10)) was increased. This was achieved by increasing the intensity parameter  $k_p$  in Eq. (13) five-fold to a value of 0.5. Results from the simulation are presented in Fig. 9j, where it is clear that increasing the sensitivity effectively closes down the network. Even with continued perfusion over a long time-scale, the capillaries fail to dilate and no stable, high conductance pathway emerges from the interconnected network. This could prove to be another important therapeutic target—by manipulating the sensitivity of ECs to WSS through their sensitivity to intravascular pressure, it may be possible to shut down the capillary bed supplying blood to a developing tumour and effectively starve it of essential nutrients.

The issues of nutrient supply and drug delivery will be considered in the following section.

## 4. Transport through adapted networks: implications for nutrient supply and drug delivery to solid tumours

In the previous section, the effects of varying a wide variety of physical and biochemical parameters upon

vascular architecture were investigated in the context of DATIA. These included investigating the network structure sensitivities to shear-induced branching, blood haematocrit, cell–matrix interactions (via the haptotaxis coefficient) and intravascular pressure. The aim of the work presented in this section is to quantify the efficiency of these different networks in carrying blood-borne material, e.g. nutrients, chemotherapy drugs, to the tumour. In doing so, it is hoped that some insights can be offered into the precise fate of chemotherapeutic agents in the vasculature during treatment and that this could lead to the identification of a number of new therapeutic targets and strategies for tumour management. This approach, through the current dynamic adaptive model for tumour-induced angiogenesis, provides a rational biomechanical basis to investigate an effect which was first reported over 30 years ago—that of drug-induced normalization of tumour blood vessels—and which has recently been the subject of renewed interest (Salsbury et al., 1970; Le Serve and Hellmann, 1972; Jain, 2001; Hellmann, 2003; Hellmann, 2004; Jain, 2004).

In order to assess transport efficacy within a given adapted vessel network, a “tracer-drug” at concentration  $C_{max}$  was continuously infused into the inlet of the parent vessel for 500 s. At each time step, the total amount of drug flowing into each capillary junction (node) was calculated, perfect mixing was assumed at each node in the network,

and new drug concentrations were calculated for all outflow bonds based upon the updated nodal values.

The base-case simulation for transport utilized the vasculature described in Section 3.4 (and shown in Fig. 7) i.e. a fully adaptive network that includes shear-induced branching. Fig. 11 shows the tracer-drug evolution through the capillary network at a number of different times (in s). It is immediately clear that the bulk (in fact, almost all) of the injected tracer-drug flows through the highly conductive dilated backbone, largely by-passing the tumour and recirculating to the parent vessel. In excess of 250 s of continuous infusion is required before any tracer-drug reaches the tumour surface, and only then in very small concentrations.

Fig. 12 shows plots of the total drug mass in the system (parent vessel and capillary network) and uptake by the tumour as functions of time. It should be noted that, (i) tumour uptake is considered to be instantaneous once the tracer-drug reaches the lower boundary of the domain, and (ii) all masses have been normalized to the total mass injected into the parent vessel over the course of the simulation. Only around 1.5% of the infused tracer-drug even enters the capillary network and, although the total mass in the network reaches a plateau after approximately 50 s (transport being essentially governed by steady-state flow through the dilated backbone), it takes another 200–250 s before uptake commences. This is because

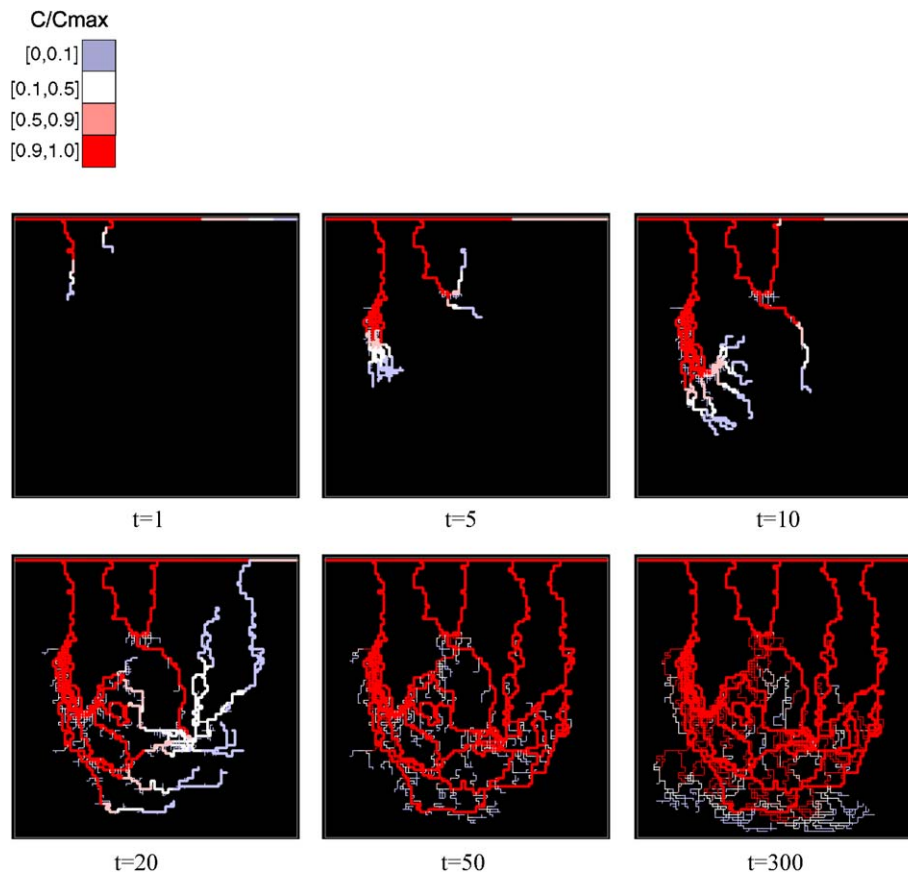


Fig. 11. Plots of the tracer-drug concentration distribution in the network shown in Fig. 7 at different times.

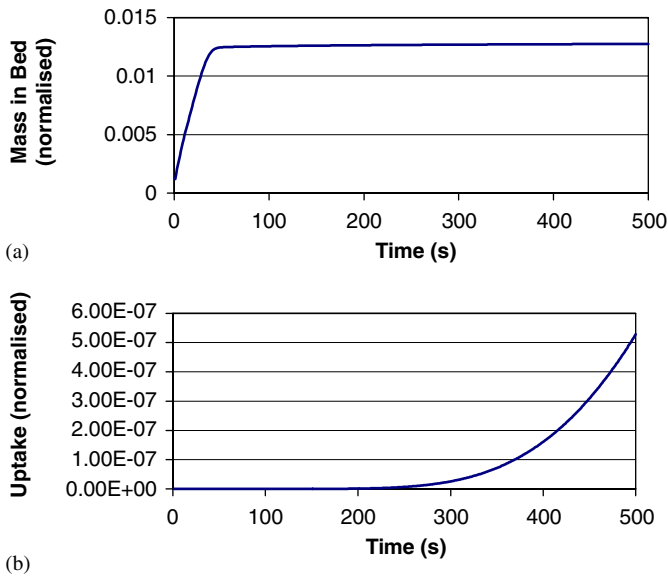


Fig. 12. Plots of (a) total drug mass in parent vessel and network over time and (b) amount of drug reaching the tumour.

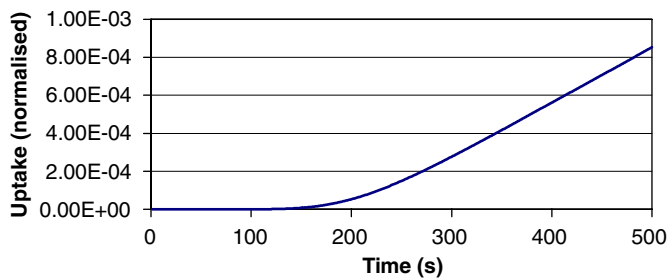


Fig. 13. Plots showing the amount of drug reaching the tumour over time in a network where all vessels have a fixed radius of  $6\mu\text{m}$ . Note the difference in scale compared to that of Fig. 12b.

capillaries forming part of the brush border close to the tumour surface are narrow and poorly perfused—consequently, only a very small fraction of the injected treatment actually reaches the target. As an aside, it should be noted that, although convective transport through the vessels of the network would be a rather poor delivery mechanism for large molecules (i.e. cytotoxic treatments), the dilated network is sufficiently well developed within a few hundred microns of the tumour surface that diffusion of nutrients (oxygen, glucose) would be relatively efficient over the time-scale of tumour growth.

Fig. 13 shows the uptake using an identical network architecture but with all capillary radii set permanently to  $6\mu\text{m}$  (the default value given at vessel birth in the model)—uptake values are approximately three orders of magnitude larger than those obtained from the remodelled vasculature. These results clearly demonstrate the impact of network heterogeneity upon treatment efficacy and highlight the need for incorporating vessel adaptations (dilation/constriction) into any angiogenesis model involving transport issues, such as chemotherapeutic intervention. In the

absence of vessel size variation, delivery is greatly overestimated.

The next example of convective transport considers flow in the capillary network produced in Fig. 8, which exhibits extensive vessel branching close to the parent vessel due to increased sensitivity to WSS. Tracer-drug concentration profiles are presented in Fig. 14 and it is apparent that the highly dilated arcades proximal to the parent vessel remove any possibility of effective treatment via intravenous or intra-arterial infusion (no delivery occurred during the 500s infusion period). However, if a tumour-induced capillary network could be forced to develop in such a way by means of some clinical intervention, then nutrient supply via diffusion could be considerably slowed and tumour growth effectively curtailed.

Another possible therapeutic target discussed earlier was the manipulation of the haptotactic response of the migrating ECs during angiogenesis. A reduction in haptotaxis led to the capillary network shown in Fig. 9c, characterized by reduced lateral migration of the vessels and reduced shear-induced branching. The tracer-drug evolution through this vessel network is shown in Fig. 15 and suggests that tumours supplied by this type of vasculature would be well supplied with nutrients and could be expected to grow rapidly. Paradoxically, however, such tumours would also be highly susceptible to infused treatments, with far more cytotoxic agent reaching the tumour than observed in previous cases. This conjecture is supported by the supply and uptake results from the infusion simulation shown in Fig. 16. Whilst the total mass of tracer-drug entering the supplying vasculature is almost identical to that observed in the base-case simulation ( $\rho = 0.28$ , Fig. 12(a)), the drug uptake by the tumour is *fifty times greater* when lateral migration and vessel branching are reduced.

The sensitivity of adaptive dynamic angiogenesis to a number of blood properties was discussed earlier in Section 3.7 and it was found that neither elevated plasma viscosity nor elevated haematocrit affected network topology to any great extent. However, a depressed haematocrit was found to lead to the formation of highly dilated arcades close to the parent vessel and Fig. 17 shows the therapeutic implications of this phenomenon—more drug enters the capillary network than entered in the base-case simulation but drug delivery to the tumour is *reduced by more than three orders of magnitude*.

The overall effect is similar to that observed when the sensitivity of the ECs to shear stress was increased. In the context of nutrient supply to the tumour, it is proposed here that decreasing local haematocrit could be a possible mechanism for generating vasculatures that are detrimental to tumour growth.

The final set of simulations dealing with nutrient and drug transport relate to networks generated under a variety of intravascular pressure conditions (i.e. the networks shown in Figs. 9g–i (the network shown in Fig. 9j clearly supplies little drug/nutrient and is not considered further).

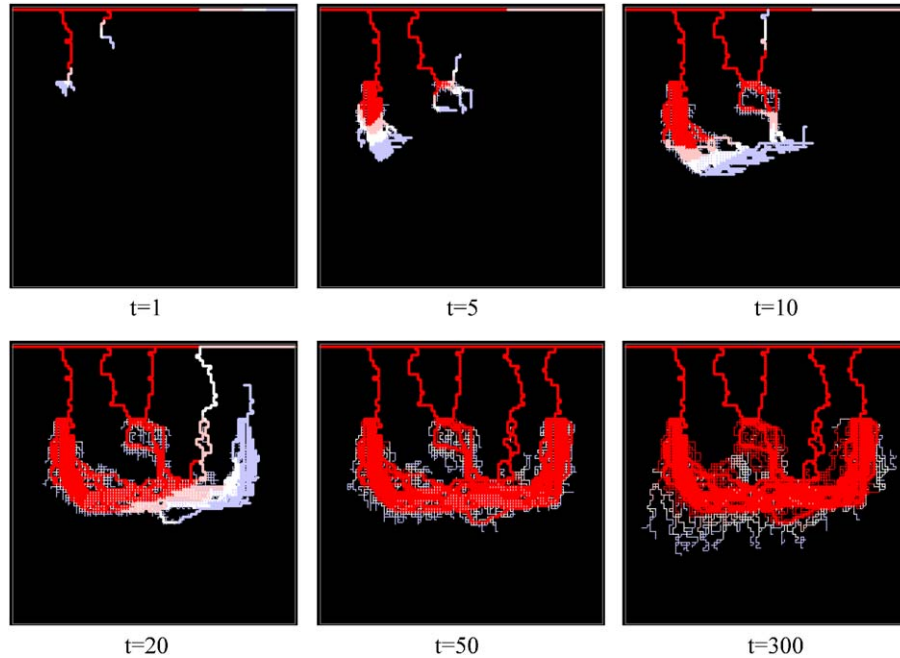


Fig. 14. Plots of the tracer-drug distribution within a capillary network where there is increased sensitivity to WSS, i.e. the network of Fig. 8.

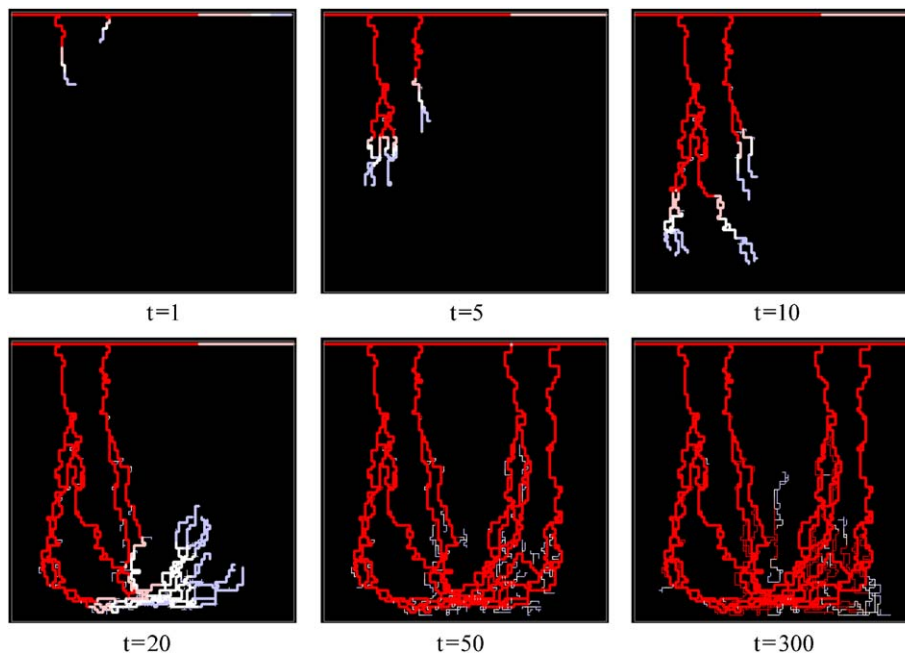


Fig. 15. Plots of the tracer-drug distribution within a capillary network developed using a reduced haptotaxis coefficient of  $\rho = 0.16$ .

Note that, in all cases, a pressure drop of 1200 Pa (9 mmHg) was applied across the parent vessel when modelling the injection of tracer-drug post-angiogenesis. Although pressure conditions used in the development of the network during angiogenesis may have differed from this, maintaining this gradient allows meaningful comparisons to be made across all simulations.

Fig. 18(a) shows uptake for the case when both inlet and outlet parent vessel pressures were reduced by 300 Pa (2.25 mmHg) prior to angiogenesis. The result, as expected,

is in broad agreement with the base-case data (Fig. 12(b)), due to the fact that both networks are structurally similar.

The impact upon drug delivery of lowering the pressure at the inlet of the parent vessel by 300 Pa (2.25 mmHg) prior to angiogenesis, whilst keeping the outlet pressure unchanged, is shown in Fig. 18(b). Delivery is dramatically increased—by more than three orders of magnitude—and tumours characterized by similar vascular architectures are consequently highly likely to be vulnerable to chemotherapeutic infusions.

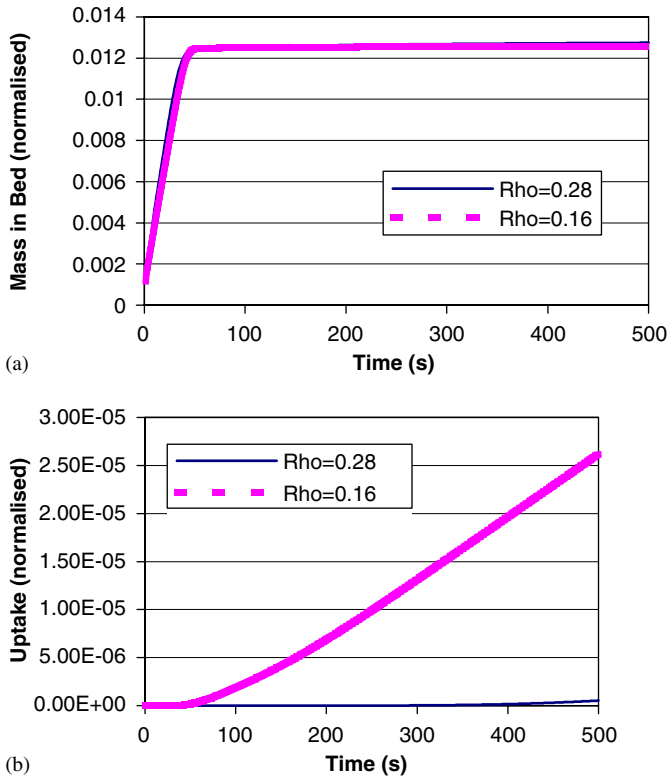


Fig. 16. Plots of (a) total drug mass in parent vessel and network over time and (b) amount of drug reaching the tumour in two different capillary networks. One network produced using a haptotaxis coefficient of  $\rho = 0.28$ , the other with a reduced haptotaxis coefficient of  $\rho = 0.16$ .

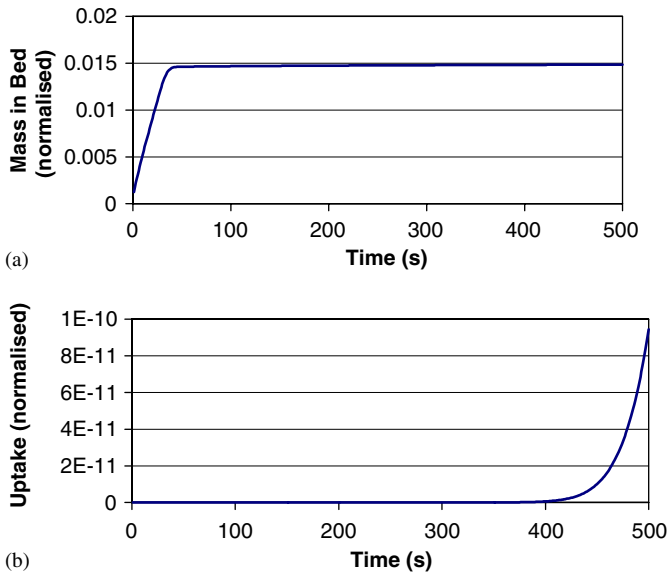


Fig. 17. Plots of (a) total drug mass in parent vessel and network over time and (b) amount of drug reaching the tumour. Capillary network produced using a reduced haematocrit value.

The final result concerning the sensitivity of angiogenesis to pressure conditions is that presented in Fig. 18(c). This figure shows the uptake by the tumour supplied by the network in Fig. 9i, where the pressure gradient across the parent vessel was increased by 300 Pa (2.25 mmHg) prior to

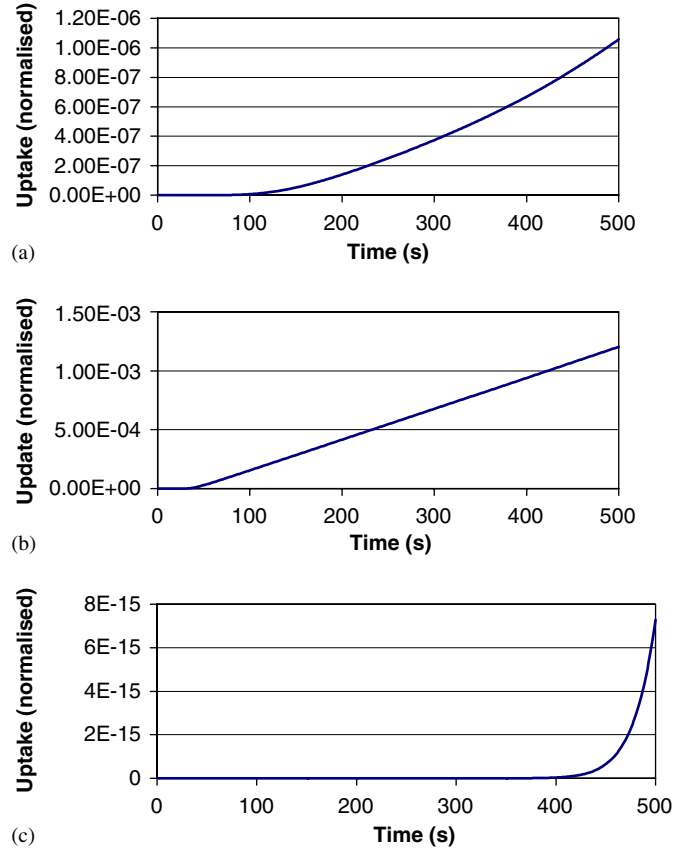


Fig. 18. Plots of amount of drug reaching the tumour in three different networks under different pressure configurations in the parent vessel. (a) Reduced inlet and outlet pressures at parent vessel; (b) lower pressure at inlet parent vessel; (c) increased pressure gradient across parent vessel.

angiogenesis. Uptake is extremely poor, which is not too surprising given the presence of highly dilated loops close to the parent vessel. Hence, intravenous/intra-arterial treatments would be expected to prove ineffective in this case.

### 5. Discussion and conclusions

An extensive theoretical investigation of the process of tumour-induced angiogenesis has been presented in this paper and results from computational simulations of the mathematical model have highlighted a number of important new targets for therapeutic intervention. The approach considered has been to integrate and explicitly couple a hybrid model of endothelial cell migration (Anderson and Chaplain, 1998) with a network flow model (McDougall et al., 2002; Stéphanou et al., 2005, 2006) and to evaluate the effects of blood perfusion and radial adaptation on the developing capillary bed. Following the work of Pries and co-workers, blood rheological properties and metabolic constraints have been explicitly included in the formulation (Pries et al., 1996, 1998, 2001a, b) and the influence of WSS on vessel branching has also been considered. In contrast to previous capillary network flow models reported in the literature (McDougall et al., 2002;

Alarcon et al., 2003; Stéphanou et al., 2005, 2006), where the effects of perfusion were evaluated a posteriori post-angiogenesis through hollow networks, blood flow in the model described here has been coupled directly to migration. Consequently, the major role played by perfusion during capillary growth has been evaluated, with radial adaptations and vessel remodelling occurring as immediate consequences of primary loop formations (anastomoses).

As a first step towards the development and implementation of the fully dynamic adaptive model, attention initially focussed upon vessel adaptation in the context of an already fully formed, flowing vascular network. Capillary vessels were considered to be devoid of red blood cells and a constant input level of haematocrit was set at the inlet end of the parent vessel. Subsequent a posteriori remodelling of the network was found to be characterized by fluctuations in vessel and network architecture, with some regions of the vasculature undergoing successive cycles of dilation and constriction in certain vessels. The network reached steady state after approximately 300 s of perfusion and the architecture was dominated by a well-defined “optimal” flow-path, consisting of a few fully dilated vessels (a flowing “backbone”), the structure of which essentially determined the efficacy of convective delivery to the tumour.

The next stage in the model development was to consider vessel adaptation during growth. This was achieved by flowing the developing network at regular intervals during the growth process until a steady-state vessel structure had been realized. However, in the absence of shear-induced branching, the network architecture and the distribution of capillary radii (i.e. vessel size) throughout the network were, as expected, found to be identical to those obtained from the a posteriori remodelling simulation.

The final development of the fully dynamic, adaptive flow model was the inclusion of shear-induced capillary branching, which enabled us to couple the flow properties directly to the growing network. This explicit coupling led to network architectures that differed radically from those found in all previous models. Dilated loops (anastomoses) formed at an earlier stage close to the parent vessel and this dilation was positively reinforcing, with proximally dilated capillaries undergoing further vessel branching. Subsequent migration of these additional branches resulted in high capillary densities in regions distal to the parent vessel and the main consequence of this was that the number of high-conductivity pathways became greatly reduced close to the tumour surface.

Computational simulation results pertaining to the sensitivity of the ECs to WSS clearly showed that this aspect of the underlying biology is an important determinant of network topology. Simulations demonstrated that manipulating the parameters relating to the degree of sensitivity to WSS could prove to be an important therapeutic target, as networks characterized by increased capillary branching would be poorly suited to supplying

nutrients to a developing tumour. Conversely, however, it was also shown that any chemotherapy treatment targeting tumour cells by injection into such a capillary network would yield poor treatment efficacy—the highly dilated shunt effectively removing any drug from the network before it had time to reach the tumour. Clearly, additional experimental research would be highly desirable to help elucidate and quantify the mechanisms whereby shear-induced branching occurs—the chemical mediators involved, the role played by convective transport, and the sensitivity of ECs to the associated signalling molecules. The implications for therapeutic intervention could then be more fully evaluated.

Additional computational simulations were carried out to investigate the sensitivity of the model to changes in a number of physical and biochemical parameters and to examine the way in which these changes affected the vascular architecture. These included sensitivities to changes in cell–matrix interactions (via the haptotaxis coefficient), blood rheological properties and intravascular pressure. The main results are summarized below:

- *Cell–matrix interactions*: Lowering the haptotactic response of the ECs caused the capillary vessels to grow towards the tumour surface more directly, with a reduction in lateral migration. This more directed motion in turn was seen to delay the formation of loops (anastomoses) and hence perfusion from the parent vessel. Vessel dilation was also delayed and only a small amount of shear-induced branching occurred. The final steady-state flowing network was somewhat ramified compared with that obtained using a higher haptotactic response and dilated pathways only emerged close to the tumour surface. This result highlighted the link between perfusion, capillary remodelling, and the underlying biological processes, emphasizing the way in which several apparently unconnected phenomena can interact throughout the process.
- *Rheological properties*: Simulations examining the role played by blood rheological properties showed that modifying plasma viscosity would not appreciably affect the final network structure after angiogenesis. However, the effect of varying haematocrit was less straightforward to predict. This was due to the fact that a number of controlling variables (radial perturbations, relative viscosity, intravascular pressure, WSS and capillary flow) are affected by variations in haematocrit simultaneously. Hence, there is no way of predicting a priori, what effect changing input haematocrit may have upon the developing vasculature. Results suggested that increasing input haematocrit above the physiological norm would have little effect upon angiogenesis, whilst a reduction in haematocrit could lead to the formation of highly dilated loops close to the parent vessel.
- *Intravascular pressure*: The final set of parameter changes presented in the paper examined the related issues of intravascular pressure and the pressure drop

across the parent vessel. Decreasing the pressure at the inlet, whilst keeping the outlet pressure fixed, led to a reduction in all capillary flows. Vessel branching consequently diminished and the vessel architecture of the resulting steady-state flowing network was seen to be less dense than before. The final architecture was similar to that obtained by reducing the haptotactic coefficient and this again emphasizes the way in which perfusion can affect the interpretation of the underlying biological processes in an unexpected manner. Decreasing blood pressure at the outlet of the parent vessel, whilst keeping the inlet pressure fixed, led to an increase in pressure gradients throughout the capillary bed and the density of shear-induced branching rose accordingly. Heavily dilated arcades formed close to the parent vessel and were reminiscent of those obtained when decreasing haematocrit or increasing the sensitivity of ECs to shear-induced branching. The final sensitivity to pressure conditions concerned the sensitivity of the capillaries to the intravascular pressure stimulus. It was found that increasing the intensity parameter  $k_p$  effectively closed down the network. Even with continued long-term perfusion, the capillaries failed to dilate and no stable, high-conductance pathway could be obtained. It was hypothesized that by manipulating the sensitivity of ECs to WSS through their sensitivity to intravascular pressure, it may be possible to shut down the capillary network supplying blood to a developing tumour and effectively starve it of essential nutrients.

In order to assess transport efficacy in the various vasculatures (and hence nutrient and drug supply to the tumour), we carried out a number of computational simulations in which a “tracer-drug” was continuously infused into the inlet of the parent vessel. In all cases, it was found that the bulk (in fact, almost all) of the injected tracer-drug flowed preferentially through the highly conductive, fully dilated vessels, largely by-passing the tumour and re-circulating to the parent vessel. Moreover, capillaries forming part of the brush border close to the tumour surface were so narrow and poorly perfused that only a very small fraction of the tracer-drug actually reached the target. Delivery of the tracer-drug to the tumour via a capillary network characterized by an identical architecture but with all vessel radii set to a mean physiological value, was overestimated by almost three orders of magnitude. These results show the impact of vessel heterogeneity within a given network upon treatment efficacy and highlight the need for incorporating vessel adaptations into any angiogenesis model involving transport issues, such as chemotherapeutic intervention.

One possible therapeutic target discussed earlier was the manipulation of the haptotactic response of the migrating ECs during angiogenesis. The tracer-drug evolution results suggest that tumours supplied by this type of vasculature would be well supplied with nutrients and could be expected to grow rapidly. Paradoxically, however, such

tumours would also be highly susceptible to infused treatments, with far more cytotoxic agent reaching the proliferating tumour rim than observed in previous cases. Indeed, tracer-drug uptake by the tumour is 50 times greater when lateral migration and vessel branching are reduced.

More generally, it is apparent from the transport simulations presented here that highly dilated loops proximal to the parent vessel remove any possibility of effective treatment via intravenous or intra-arterial infusion. However, if a tumour-induced capillary network could be forced to develop in just such a way, by means of some clinical intervention perhaps, then nutrient supply to the tumour could be effectively curtailed. The DATIA model provides a solid biomechanical framework within which to examine, in some detail, the possibility of normalizing tumour blood vessels as a means of effectively treating solid tumours (cf. Salsbury et al., 1970; Le Serve and Hellmann, 1972).

### Acknowledgements

This work was partly supported by the European Community, through the Marie Curie Research Training Network Project HPRN-CT-2004-503661: “*Modelling, Mathematical Methods and Computer Simulation of Tumour Growth and Therapy*”.

### References

- Alarcon, T., Byrne, H., Maini, P., 2003. A cellular automaton model for tumour growth in inhomogeneous environment. *J. Theor. Biol.* 225 (2), 257–274.
- Anderson, A.R.A., 2005. A hybrid mathematical model of solid tumour invasion: the importance of cell adhesion. *Math. Med. Biol.* 22, 163–186.
- Anderson, A.R.A., Chaplain, M.A.J., Newman, E.L., Steele, R.J.C., Thompson, A.M., 2000. Mathematical modelling of tumour invasion and metastasis. *J. Theor. Med.* 2, 129–154.
- Anderson, A.R.A., Chaplain, M.A.J., 1998. Continuous and discrete mathematical models of tumor-induced angiogenesis. *Bull. Math. Biol.* 60, 857–899.
- Ausprunk, D.H., Folkman, J., 1977. Migration and proliferation of endothelial cells in preformed and newly formed blood vessels during tumour angiogenesis. *Microvasc. Res.* 14, 53–65.
- Baish, J.W., Gazit, Y., Berk, D.A., Nozue, M., Baxter, L.T., Jain, R.K., 1996. Role of tumor vascular architecture in nutrient and drug delivery: an invasion percolation-based network model. *Microvasc. Res.* 51, 327–346.
- Benjamin, L.E., Hemo, I., Keshet, E., 1998. A plasticity window for blood vessel remodelling is defined by pericyte coverage of the preformed endothelial network and is regulated by PDGF- $\beta$  and VEGF. *Development (Camb.)* 125, 1591–1598.
- Bray, D., 1992. *Cell Movements*. Garland Publishing, New York.
- Carmeliet, P., 2003. Angiogenesis in health and disease. *Nature Med.* 9, 653–660.
- Ciofalo, M., Collins, M.W., Hennessy, T.R., 1999. Microhydrodynamics phenomena in the circulation. In: Mala, N. (Ed.), *Nanoscale Fluid Dynamics in physiological Processes, A Review Study*. WIT Press, pp. 219–236.
- Cleaver, O., Melton, D.A., 2003. Endothelial signaling during development. *Nature Med.* 9, 661–668.

- Davis, G.E., Pintar Allen, K.A., Salazar, R., Maxwell, S.A., 2000. Matrix metalloproteinase-1 and -9 activation by plasmin regulates a novel endothelial cell-mediated mechanism of collagen gel contraction and capillary tube regression in three-dimensional collagen matrices. *J. Cell Sci.* 114, 917–930.
- El-Kareh, A.W., Secomb, T.W., 1997. Theoretical models for drug delivery to solid tumours. *Crit. Rev. Biomed. Eng.* 25 (6), 503–571.
- Ferrara, N., Gerber, H.-P., LeCouter, J., 2003. The biology of VEGF and its receptors. *Nature Med.* 9, 669–676.
- Fisher, A.B., Chien, S., Barakat, A.I., Nerem, R.M., 2001. Endothelial cellular response to altered shear stress. *Am. J. Physiol. Lung Cell Mol. Physiol.* 281, L529–L533.
- Folkman, J., 1971. Tumor angiogenesis: therapeutic implications. *Nature Engl. J. Med.* 285, 1182–1186.
- Folkman, J., 1995. Angiogenesis in cancer, vascular, rheumatoid and other disease. *Nature Med.* 1, 21–31.
- Folkman, J., Klagsbrun, M., 1987. Angiogenic factors. *Science* 235, 442–447.
- Fung, Y.C., 1993. *Biomechanics*. Springer, New York.
- Gee, M.S., Procopio, W.N., Makonnen, S., Feldman, M.D., Yeilding, N.M., Lee, M.F., 2003. Tumor vessel development and maturation impose limits on the effectiveness of anti-vascular therapy. *Am. J. Pathol.* 162, 183–193.
- Gimbrone, M.A., Cotran, R.S., Leapman, S.B., Folkman, J., 1974. Tumor growth and neovascularization: an experimental model using the rabbit cornea. *J. Natl. Cancer Inst.* 52, 413–427.
- Godde, R., Kurz, H., 2001. Structural and biophysical simulation of angiogenesis and vascular remodeling. *Dev. Dynam.* 220, 387–401.
- Hellmann, K., 2003. Dynamics of tumour angiogenesis: effect of razoxane-induced growth rate slowdown. *Clin. Exp. Metastas.* 20, 95–102.
- Hellmann, K., 2004. Recognition of tumor blood vessel normalization as a new antiangiogenic concept. *Nature Med.* 10, 329.
- Hidalgo, M., Eckhardt, S.G., 2001. Development of matrix metalloproteinase inhibitors in cancer therapy. *J. Natl. Cancer Inst.* 93, 178–193.
- Jain, R.K., 1987. Transport of molecules in the tumor interstitium: a review. *Cancer Res.* 47 (12), 3039–3051.
- Jain, R.K., 1988. Determinants of tumour blood flow: a review. *Cancer Res.* 48 (10), 2641–2658.
- Jain, R.K., 2001. Normalizing tumor vasculature with anti-angiogenic therapy: a new paradigm for combination therapy. *Nature Med.* 7, 987–989.
- Jain, R.K., 2003. Molecular regulation of vessel maturation. *Nature Med.* 9, 685–693.
- Jain, R.K., 2004. Recognition of tumor blood vessel normalization as a new antiangiogenic concept. *Nature Med.* 10, 329–330.
- Kamiya, A., Bukhari, R., Togawa, T., 1984. Adaptive regulation of wall shear stress optimizing vascular tree function. *Bull. Math. Biol.* 46, 127–137.
- Krenz, G.S., Dawson, C.A., 2002. Vessel distensibility and flow distribution in vascular trees. *J. Math. Biol.* 44, 360–374.
- Le Serve, A.W., Hellmann, K., 1972. *Br. Med. J.* 1, 597–601.
- Lehoux, S., Tedgui, A., 1998. Signal transduction of mechanical stresses in the vascular wall. *Hypertension* 32, 338–345.
- Levine, H.A., Pamuk, S., Sleeman, B.D., Nielsen-Hamilton, M., 2001. Mathematical modeling of the capillary formation and development in tumor angiogenesis: penetration into the stroma. *Bull. Math. Biol.* 63 (5), 801–863.
- Levine, H.A., Tucker, A.L., Nielsen-Hamilton, M., 2002. A mathematical model for the role of cell signal transduction in the initiation and inhibition of angiogenesis. *Growth Factors* 20 (4), 155–175.
- Lolas, G., 2003. Mathematical modelling of the urokinase plasminogen activator system and its role in cancer invasion of tissue. Ph.D. Thesis, University of Dundee.
- Mantzaris, N.V., Webb, S., Othmer, H.G., 2004. Mathematical modeling of tumor-induced angiogenesis. *J. Math. Biol.* 49, 111–187.
- McDougall, S.R., Sorbie, K., 1997. The application of network modelling techniques to multiphase flow in porous media. *Petrol. Geosci.* 3, 161–169.
- McDougall, S.R., Anderson, A.R.A., Chaplain, M.A.J., Sherratt, J.A., 2002. Mathematical modelling of flow through vascular networks: implications for tumour-induced angiogenesis and chemotherapy strategies. *Bull. Math. Biol.* 64 (4), 673–702.
- Morikawa, S., Baluk, P., Kaidoh, T., Haskell, A., Jain, R.K., McDonald, D.M., 2002. Abnormalities in pericytes on blood vessels and endothelial sprouts in tumors. *Am. J. Pathol.* 160, 985–1000.
- Muthukkaruppan, V.R., Kubai, L., Auerbach, R., 1982. Tumor-induced neovascularization in the mouse eye. *J. Natl. Cancer Inst.* 69, 699–705.
- Olsen, L., Sherratt, J.A., Maini, P.K., Arnold, F., 1997. A mathematical model for the capillary endothelial cell-extracellular matrix interactions in wound-healing angiogenesis. *IMA J. Math. Appl. Med. Biol.* 14, 261–281.
- Orme, M.E., Chaplain, M.A.J., 1997. Two-dimensional models of tumour angiogenesis and anti-angiogenesis strategies. *IMA J. Math. Appl. Med. Biol.* 14, 189–205.
- Paweletz, N., Knierim, M., 1989. Tumor-related angiogenesis. *Crit. Rev. Oncol. Hematol.* 9, 197–242.
- Plank, M.J., Sleeman, B.D., 2004. Lattice and non-lattice models of tumour angiogenesis. *Bull. Math. Biol.* 66, 1785–1819.
- Pries, A.R., Secomb, T.W., Gaehtgens, P., 1996. Biophysical aspects of blood flow in the microvasculature. *Cardiovasc. Res.* 32, 654–667.
- Pries, A.R., Secomb, T.W., Gaehtgens, P., 1998. Structural adaptation and stability of microvascular networks: theory and simulation. *Am. J. Physiol. Heart Circ. Physiol.* 275 (44), H349–H360.
- Pries, A.R., Reglin, B., Secomb, T.W., 2001a. Structural adaptation of microvascular networks: functional roles of adaptive responses. *Am. J. Physiol. Heart Circ. Physiol.* 281, H1015–H1025.
- Pries, A.R., Reglin, B., Secomb, T.W., 2001b. Structural adaptation of vascular networks: role of the pressure response. *Hypertension* 38, 1476–1479.
- Pugh, C.W., Ratcliffe, P.J., 2003. Regulation of angiogenesis by hypoxia: role of the HIF system. *Nature Med.* 9, 677–684.
- Quarteroni, A., Tuveri, M., Veneziani, A., 2000. Computational vascular fluid dynamics: problems, models and methods. *Comput. Visual. Sci.* 2, 163–197.
- Quick, C.M., Young, W.L., Leonard, E.F., Joshi, S., Gao, E., Hashimoto, T., 2000. Model of structural and functional adaptation of small conductance vessels to arterial hypotension. *Am. J. Physiol. Heart Circ. Physiol.* 279, H1645–H1653.
- Rafii, S., Lyden, D., 2003. Therapeutic stem and progenitor cell transplantation for organ vascularization and regeneration. *Nature Med.* 9, 702–712.
- Risau, W., 1997. Mechanisms of angiogenesis. *Nature* 386, 671–674.
- Salsbury, A.J., Burrage, K., Hellmann, K., 1970. *Br. Med. J.* 4, 344–346.
- Secomb, T.W., 1995. Mechanics of blood flow in the microcirculation. *Soc. Exp. Biol.*, 305–321.
- Sholley, M.M., Ferguson, G.P., Seibel, H.R., Montour, J.L., Wilson, J.D., 1984. Mechanisms of neovascularization. Vascular sprouting can occur without proliferation of endothelial cells. *Lab. Invest.* 51, 624–634.
- Stéphanou, A., McDougall, S.R., Anderson, A.R.A., Chaplain, M.A.J., 2005. Mathematical modelling of flow in 2D and 3D vascular networks: applications to anti-angiogenic and chemotherapeutic drug strategies. *Math. Comp. Model.* 41, 1137–1156.
- Stéphanou, A., McDougall, S.R., Anderson, A.R.A., Chaplain, M.A.J., 2006. Mathematical modelling of the influence of blood rheological properties upon adaptive tumour-induced angiogenesis. *Math. Comp. Model.*, to appear.
- Sternlicht, M.D., Werb, Z., 2001. How matrix metalloproteinases regulate cell behavior. *Annu. Rev. Cell Dev. Biol.* 17, 463–516.
- Stokes, C.L., Lauffenburger, D.A., 1991. Analysis of the roles of microvessel endothelial cell random motility and chemotaxis in angiogenesis. *J. Theor. Biol.* 152, 377–403.
- Taber, L.A., 1998. An optimization principle for vascular radius including the effects of smooth muscle tone. *Biophys. J.* 74, 109–114.

- Thompson, D.W., 1917. *On Growth and Form*. Cambridge University Press, Cambridge.
- Walsh, D.A., 1999. Angiogenesis and arthritis. *Rheumatology* 38, 103–112.
- Yan, L., Moses, M.A., Huang, S., Ingber, D., 2000. Adhesion-dependent control of matrix metalloproteinase-2 activation in human capillary endothelial cells. *J. Cell Sci.* 113, 3979–3987.
- Ylä-Herttuala, S., Alitalo, K., 2003. Gene transfer as a tool to induce therapeutic vascular growth. *Nature Med.* 9, 694–701.

### **Further reading**

- Ergun, S., Kilic, N., Wurmbach, J.H., Ebrahimnejad, A., Fernando, M., Sevinc, S., Kilic, E., Chalajour, F., Fiedler, W., Lauke, H., Lamszus, K., Hammerer, P., Weil, J., Herbst, H., Folkman, J., 2001. Endostatin inhibits angiogenesis by stabilization of newly formed endothelial tubes. *Angiogenesis* 4 (3), 193–206.
- Mitchell, A.R., Griffiths, D.F., 1980. *The Finite Difference Method in Partial Differential Equations*. Wiley, Chichester.